

Perseverance MEDA Atmospheric Pressure Observations - Initial Results

Ari-Matti Harri^{1*}, Mark Paton¹, Maria Hieta¹, Jouni Polkko¹, Claire Newman², Jorge Pla-Garcia³, Joonas Leino¹, Terhi Mäkinen¹, Janne Kauhanen¹, Iina Jaakonaho¹, Agustin Sánchez-Lavega⁴, Ricardo Hueso⁴, Maria Genzer¹, Ralph Lorenz⁵, Mark Lemmon⁶, Alvaro Vicente-Retortillo³, Leslie K. Tamppari⁷, Daniel Viudez-Moreiras³, Manuel de la Torre-Juarez⁷, Hannu Savijärvi¹, Javier A. Rodríguez-Manfredi³, German Martinez⁸

¹Finnish Meteorological Institute, Helsinki, Finland

²Aeolis Research, Chandler, AZ, USA

³Centro de Astrobiología (INTA-CSIC), Madrid, Spain

⁴UPV/EHU, Bilbao, Spain

⁵Johns Hopkins Applied Physics Laboratory, Laurel, MD, USA

⁶Space Science Institute, College Station, TX, USA

⁷Jet Propulsion Laboratory/California Institute of Technology, Pasadena, CA, USA

⁸Lunar and Planetary Institute, Houston, TX, USA

Key Points:

- The atmospheric pressure observations by Perseverance Rover have proved to be of excellent quality fulfilling expectations
- Jezero crater pressure exhibits significant differences to other Martian areas likely due to varying regional geography and solar forcing
- Overall, the diurnal and seasonal atmospheric pressure cycles at Jezero Crater follow an anticipated pattern of pressure variation

*P.O. Box 503, 00101 Helsinki, Finland

Corresponding author: Ari-Matti Harri, Ari-Matti.Harri@fmi.fi

24 **Abstract**

25 The Mars2020 Perseverance Rover landed successfully on the Martian surface
 26 on the Jezero Crater floor (18.44°N, 77.45°E) at Martian solar longitude, L_s , ~ 5
 27 in February 2021. Since then it has produced highly valuable environmental measure-
 28 ments with a versatile scientific payload including the MEDA (Mars Environmental
 29 Dynamics Analyzer) suite of environmental sensors. One of the MEDA systems is
 30 the PS pressure sensor system which weighs 40 grams and has an estimated absolute
 31 accuracy of better than 3.5 Pa and a resolution of 0.13 Pa. We present initial results
 32 from the first 414 sols of Martian atmospheric surface pressure observations by the
 33 PS whose performance was found to meet its specifications. Observed sol-averaged
 34 atmospheric pressures follow an anticipated pattern of pressure variation in the
 35 course of the advancing season and are consistent with data from other landing mis-
 36 sions. The observed diurnal pressure amplitude varies by ~ 2 -5 % of the sol-averaged
 37 pressure, with absolute amplitude 10-35 Pa in an approximately direct relationship
 38 with airborne dust. During a regional dust storm, which began at L_s 135° the di-
 39 urnal pressure amplitude roughly doubles. The diurnal pressure variations were found
 40 to be remarkably sensitive to the seasonal evolution of the atmosphere. In particular
 41 analysis of the diurnal pressure signature revealed diagnostic information likely re-
 42 lated to the regional scale structure of the atmosphere. Comparison of Perseverance
 43 pressure observations to data from other landers reveals the global scale seasonal
 44 behaviour of Mars' atmosphere.

45 **Plain Language Summary**

46 The Mars2020 Perseverance Rover successfully arrived at Mars in February
 47 2021. It landed during an early Martian spring afternoon in a crater north of Mars'
 48 equator called Jezero crater. The rover is equipped with meteorological instruments
 49 that have so far produced extensive and valuable data for understanding the Mar-
 50 tian atmosphere. One of the meteorological instruments is an accurate and precise
 51 pressure sensor. The pressure sensor has revealed large changes in the pressure over
 52 the seasons that are related to large changes in the actual mass of the Martian at-
 53 mosphere. This is in line with seasonal pressure changes measured during previous
 54 Mars missions and can be explained as the freezing of the atmosphere onto the
 55 Martian poles and its subsequent thaw. On a shorter time scale the pressure sensor
 56 revealed complex pressure changes over a Martian day. These variations are thought
 57 to be related to atmospheric dust whose ubiquitous nature is known to have a strong
 58 influence on the Martian climate. As the seasons progressed the daily pressure vari-
 59 ations morphed to exhibit different patterns likely related to the large-scale regional
 60 changes in the atmosphere. Comparison of Perseverance pressure observations to
 61 other landers revealed the global nature of the atmosphere.

62 **1 Introduction**

63 The Mars2020 Perseverance Rover landed successfully on the Martian sur-
 64 face on the Jezero Crater floor (18.44°N, 77.45°E) at the Martian solar longitude,
 65 L_s , 5° in February 2021. Since then, it has produced highly valuable environmental
 66 measurements with a versatile scientific payload including the MEDA (Mars Envi-
 67 ronmental Dynamics Analyzer) suite of environmental sensors (Rodriguez-Manfredi
 68 et al., 2021). One of the MEDA sensor systems is the pressure sensor (PS) whose
 69 observations and initial results utilizing the data acquired during the first 414 sols of
 70 the mission ($L_s 5 - 212^\circ$) will be addressed in this manuscript.

71 Martian atmospheric investigations through spacecraft observations began in
 72 the early to middle 1960s as reported by, *e.g.*, Kliore et al. (1969, 1973) and later

73 by Kieffer et al. (1973, 1977); Snyder and Moroz (1992); Zurek (1992); Zurek et
74 al. (1992a). Surface pressure of the atmosphere was firstly estimated using remote
75 sensing methods, both ground based by *e.g.* (Young, 1969) and from spacecraft
76 starting from Mariner as reported by, *e.g.* (Kliore et al., 1965). The Viking landers
77 in 1974-77 provided the first time series of *in situ* atmospheric observations that
78 turned out to be a treasure trove of data covering multiple Martian years (Kieffer
79 et al., 1977; Tillman et al., 1979; Zurek, 1978, 1981). Thereafter Mars Pathfinder
80 (M. P. Golombek et al., 1999; Schofield et al., 1997), the Phoenix lander (Taylor et
81 al., 2008; Savijärvi & Määttänen, 2010), the Mars Science Laboratory aka Curiosity
82 Rover (Gómez-Elvira et al., 2012), the InSight lander (M. Golombek et al., 2020)
83 and the Perseverance Rover (Rodriguez-Manfredi et al., 2021) have continued *in situ*
84 investigations of the Martian atmosphere including accurate atmospheric pressure
85 observations.

86 During the years of *in situ* and remote observations, Martian atmospheric
87 observations have been accompanied and supplemented by increasingly sophisti-
88 cated and varied modeling efforts in a range of spatial and temporal scales already
89 since late 1960s (Leovy & Mintz, 1969; Pollack et al., 1981, 1990; Haberle et al.,
90 1993; Barnes et al., 1993; Forget et al., 1999; Richardson et al., 2007; Savijärvi &
91 Kauhanen, 2008; Newman et al., 2017; Richardson & Newman, 2018; Newman et
92 al., 2019). Pressure observations from surface stations have prompted investiga-
93 tions of the CO₂ cycle and its connection to the poles, ice and dust *e.g.* Guo et al.
94 (2009); Kahre and Haberle (2010). The characterisation of pressure changes due
95 to large scale circulations (Wilson & Hamilton, 1996; Basu et al., 2004) and local
96 meteorology (Toigo & Richardson, 2003; Rafkin et al., 2016) have been predicted
97 and characterised using computer models.

98 Data assimilation using orbital data is an important activity to enable real-
99 istic predictions using atmospheric models and verifying the physics (Rogberg et
100 al., 2010; Lee et al., 2011; Montabone et al., 2014). Better understanding of the be-
101 haviour of the Martian atmosphere can help develop better predictions *e.g.* Battalio
102 and Lora (2021). A network of surface pressure stations could be key to char-
103 acterising fast evolving weather systems and dust lifting events (Newman et al.,
104 2021). Our current understanding of the Martian atmosphere and its processes is
105 still understandably far less detailed than our understanding of our own terrestrial
106 atmosphere, but the Martian atmospheric phenomena are presently clearly much
107 better understood than those of any other solar system atmospheres.

108 Some of the earlier Martian landing vehicles have operated at similar latitudes
109 or elevations to Perseverance, resulting in similarities in terms of climate zone or
110 annual mean atmospheric pressure. Figure 1 shows the locations of Martian land-
111 ing vehicles with Martian topography, giving a clear idea of the differences in the
112 altitude and type of terrain of the landing sites. In terms of longitude, however, Per-
113 severance seems to be relatively isolated, which has implications when comparing
114 to data from other landed missions. Perseverance observations also have particular
115 significance because they mean that for the first time, we have four *in situ* sets of
116 meteorological observations being carried out at the same time at different locations
117 on the Martian surface (including observations by MSL, InSight, Perseverance, and
118 also China's Zhurong rover, data from which are not currently publicly available).
119 We will present several interesting initial discoveries based on these facts, in addition
120 to the independent Perseverance pressure observations.

121 In addition to this article there are two companion articles in this journal uti-
122 lizing the pressure data focusing on atmospheric dynamics (Sánchez-Lavega et al.,
123 2023) and small-scale thermal vortices (Hueso et al., 2023).

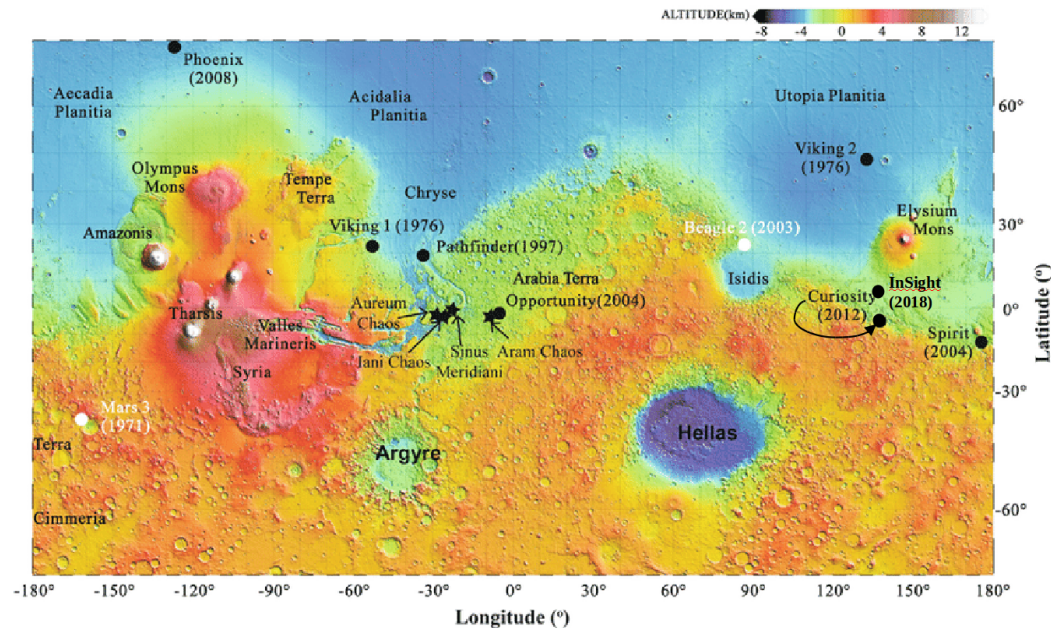


Figure 1. Landing sites of the seven spacecraft having provided *in situ* atmospheric data depicted on a topographic map of Mars (NASA JPL, 2021).

2 Brief MEDA PS device specification and performance

Instrument description. The Perseverance pressure measurement device (MEDA PS) is based on the silicon-micro-machined pressure sensor head (Barocap®) and transducer technology developed by Vaisala Inc. The Barocap® version used by MEDA PS is optimized for the Martian near-surface atmospheric pressure. Changing ambient pressure is changing the sensor head capacitance by varying the distance of the sensor head capacitor plates. Besides being pressure dependent, the Barocap® capacitance is also sensitive to temperature, and thus accurate temperature measurements close to the sensor head are necessary. The supporting house-keeping temperature measurements are provided by Vaisala’s Thermocap® sensor heads.

MEDA PS consists of two transducers, each having its controlling ASIC (application specific integrated circuit) and 8 channels containing the Barocap sensor heads, Thermocap sensor heads and constant reference capacitors. Two types of Barocap sensors are used: the NGM type with high stability and relatively long warm-up time and the less stable but faster RSP2M type as a backup. Hence, the primary sensor for scientific investigations is the NGM type Barocap on transducer 1 channel 8 and the secondary sensor the RSP2M Barocap on transducer 1 channel 6. We provide a calibrated pressure reading for both sensor heads in the DER and CAL type data products in the PDS archive (Rodriguez-Manfredi & de la Torre Juarez, 2021) that are optimal for most investigations.

Calibration and performance. MEDA PS has been calibrated at the Finnish Meteorological Institute (FMI) laboratories over the expected operational pressure and temperature ranges. The calibration has been performed in stable temperatures from -45°C to $+55^{\circ}\text{C}$ and stable pressure points ranging from 0 hPa to 14 hPa, which extend well beyond the pressure and temperature ranges prevailing within the electronics compartment housing the MEDA PS on Mars itself. Cali-

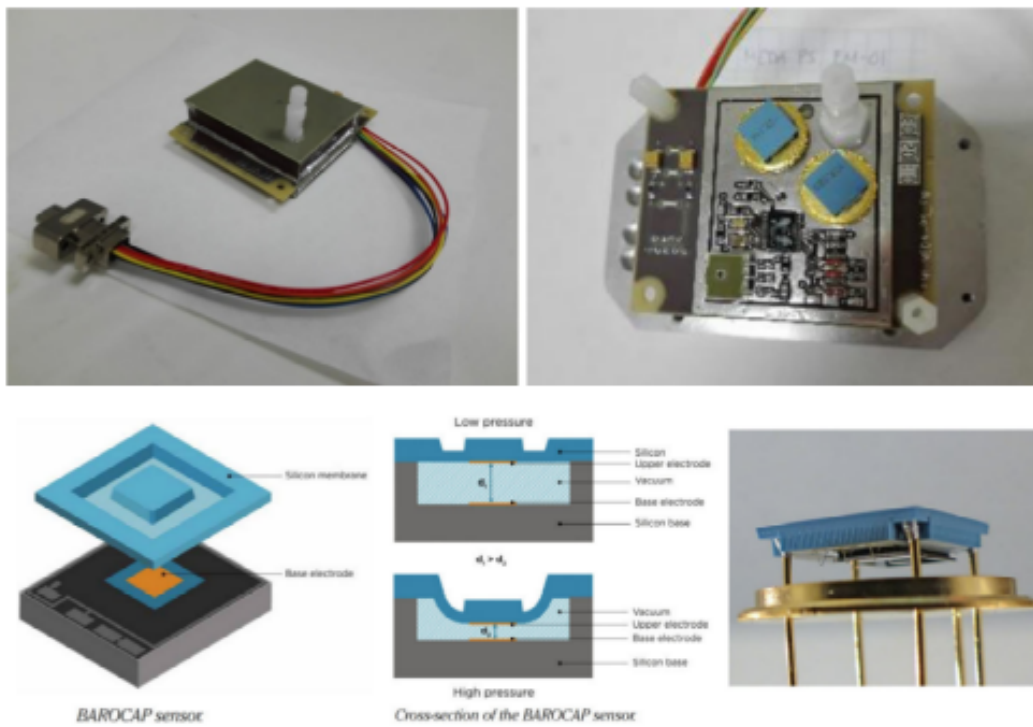


Figure 2. MEDA PS device within its Faraday cage made out of thin conductive foil (top left pane) and the instrument with its pressure sensor heads and part of the electronics visible without the Faraday cover (top right pane). The structure of the silicon micromachined sensor head is shown on the lower row.

151 bration measurements were also performed in changing pressure and temperature
 152 conditions. The Barocap sensors are known to have small changes in the tempera-
 153 ture dependence or sensor offset when introduced to a new electrical and thermal
 154 environment, and thus calibration checks were performed at all stages after the
 155 sensor-level calibration. The calibration checks were performed after integration
 156 to the MEDA electronics compartment (MEDA ICU), during the final rover-level
 157 thermal vacuum test, during the interplanetary cruise and soon after landing on
 158 Mars. The RSP2M Barocaps are also periodically cross-checked against the primary
 159 Barocap for possible drift compensation.

160 The estimated MEDA PS uncertainty based on the sensor- and rover-level
 161 measurements was analyzed to be better than 3.5 Pa. This includes the effects of
 162 the short-term repeatability, environmental effects and the pressure reference accu-
 163 racy. The resolution of the primary Barocap, restricted mostly by the electronics
 164 noise, is 0.13 Pa in nominal measurement mode, and 0.1 Pa in high-resolution mode,
 165 as determined in sensor-level measurements. According to the test data, the time
 166 response of MEDA PS is equal to or less than 1 s, having almost no effect on the
 167 measurements at the nominal sampling rate of 1 Hz. The effect of the warm-up time
 168 of the NGM Barocaps has been removed by the calibration.

169 The system resources required by the whole MEDA PS package are dimensions
 170 $62 \times 50 \times 17$ mm, mass 43 g and power consumption less than 15 mW. The MEDA
 171 PS detailed specification available before the launch of the Perseverance Rover is
 172 described in detail by (Rodriguez-Manfredi et al., 2021). The MEDA PS is located
 173 inside the MEDA Instrument Control Unit (ICU) in the rover body, with a filter-
 174 protected tube connecting it to the outside environment and conveying ambient
 175 pressure to be measured. The MEDA PS device is depicted in Figure 2 illustrat-
 176 ating the pressure sensor head and its encapsulation of the full pressure device in a
 177 Faraday cage giving shielding against electromagnetic interference.

178 During the first 414 Martian sols of Perseverance operations MEDA PS has
 179 been functioning as expected. The temperature dependence of the Barocap sensors
 180 was checked and corrected at the beginning of the operations against the primary
 181 Barocap, which is known to be very stable based on the test data. In the first drift
 182 offset check performed after 150 sols, the drift of the secondary Barocap was less
 183 than 0.3 Pa and slightly larger for the other RSP2M Barocaps.

184 3 MEDA PS observation strategy and pressure data coverage

185 MEDA has been designed for flexible operations that are being conducted
 186 according to the scheduling by the Perseverance rover. MEDA measures for five
 187 minutes at the top of each hour in local mean solar time (LMST) in every mission
 188 sol, other than during exceptional circumstances. In addition, on average, MEDA is
 189 operating continuously for every other hour. That enables us to generate data sets
 190 with averaged pressure measurements approximately at 1-hour intervals, as well as
 191 data sets with pressure observations at 1 second intervals for a period of one hour
 192 or a few hours in a row for *e.g.* turbulence-related studies. There are also periods,
 193 when MEDA is only able to measure for five minutes per hour (or sometimes fifteen
 194 or twenty minutes per hour) or is doing no measurements at all for a few hours, due
 195 to Perseverance resource allocation reasons.

196 In the present investigations we use data sets with 1-hour intervals. The 1-hour
 197 data sets are not complete but they do have gaps due to scheduling of Persever-
 198 ance and MEDA operations. Figure 3 illustrates how well the observed data sets
 199 cover each Perseverance sol. in the average about 50-70 % of the 24 hour of a sol
 200 throughout the season with some periods having 100 % coverage and few sols have

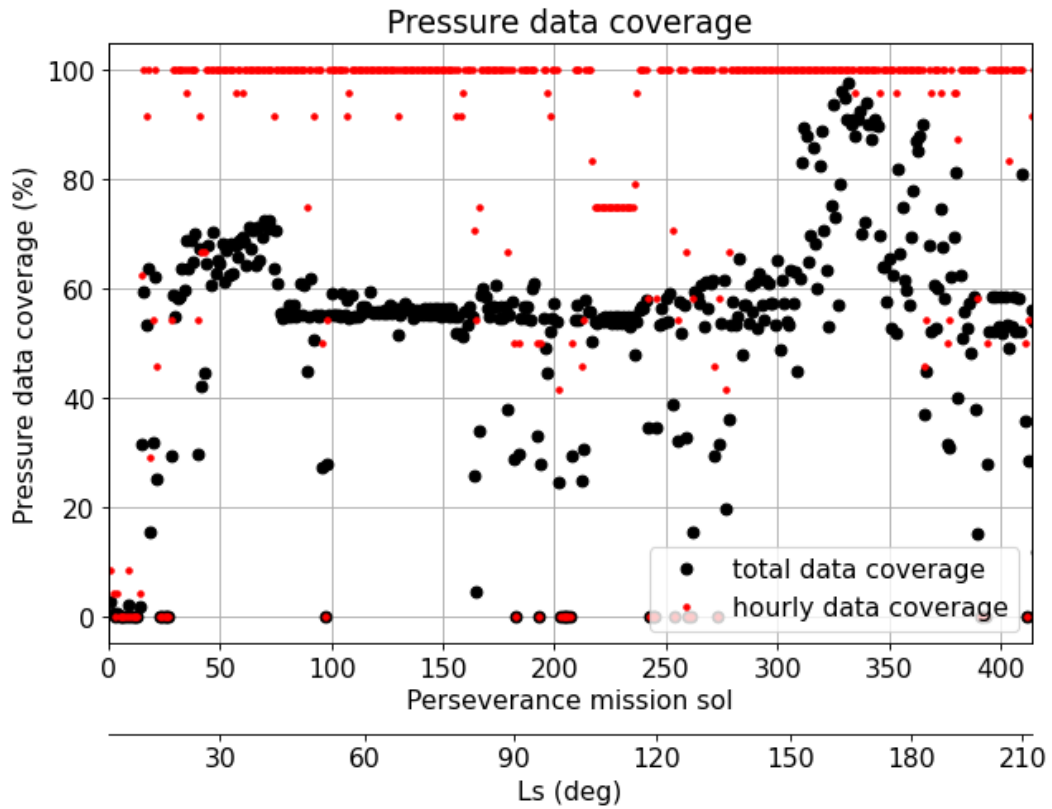


Figure 3. The coverage of atmospheric pressure observations made by the MEDA PS instrument. The black dots depict the overall percentage of pressure readings once per second in a sol, red dots the percentage of the pressure readings available at 1-hour intervals.

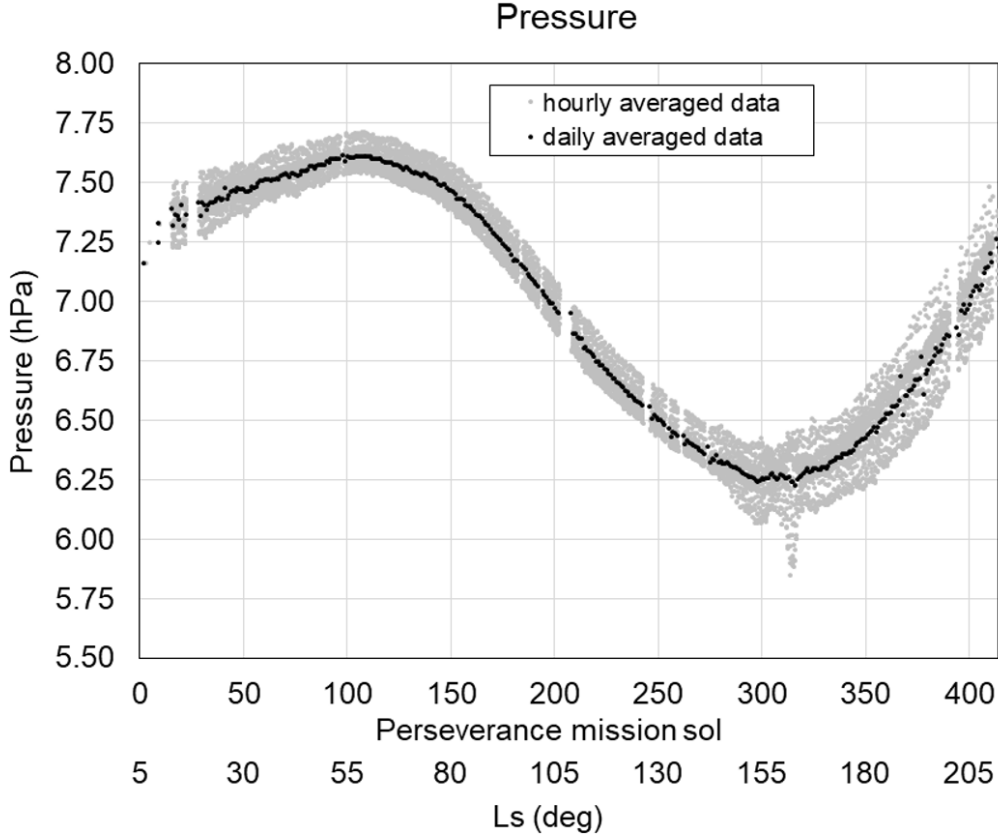


Figure 4. The sol averaged pressure data and the diurnal pressure amplitude (approximate total peak-to-peak range based on observations once per hour) for Perseverance during the period of the first 414 sols corresponding to approximately solar longitude range of L_s 5 – 212°.

201 no pressure data at all. The gaps in the 1-hour data set take place more or less ran-
 202 domly around the 24 hour Martian sol. The data coverage of this level allows good
 203 characterisation of both the diurnal and seasonal variations in the pressure.

204 **4 Changes in Jezero crater atmospheric pressure with seasonal** 205 **cycle**

206 The condensation and sublimation of CO₂ in the polar regions during win-
 207 ter and spring causes planetwide seasonal variations in the surface pressure, which
 208 were first detected by the Viking landers as reported by, *e.g.*, Kieffer et al. (1977);
 209 Tillman et al. (1979). The seasonal CO₂ cycle, which is largely controlled by the po-
 210 lar heat balance (Paige & Ingersoll, 1985, *e.g.*), can clearly be seen in the seasonal
 211 variation of daily average surface pressure.

212 This is nicely demonstrated at the Jezero crater site by the Perseverance Rover
 213 measurements. The daily averaged atmospheric surface pressure during the first 414
 214 sols of the Perseverance mission is depicted in Figure 4. The figure also includes the
 215 range of diurnal pressure variation plotted on both sides of the average pressure line
 216 with a gray color. Hence the gray area illustrates the approximate total range of di-
 217 urnal pressure variation around the average pressure of a sol. The minimum pressure

218 peak at around Ls 153 shown in Figure 4 was likely caused by a regional dust storm
219 (Lemmon et al., 2022).

220 In seasonal-to-annual time scales the CO₂ condensation-sublimation cycle at
221 the polar regions gives rise to a seasonal pressure variation on the order of as much
222 as 30 % of the local surface pressure (Kieffer et al., 1977; Tillman et al., 1979, e.g.).
223 The observed sol-averaged atmospheric pressure during the 414 first Perseverance
224 sols, from the landing time at early Northern springtime to Northern fall, follows an
225 anticipated pattern of total pressure variation in the course of the advancing sea-
226 son. The data has the first maximum in late spring roughly on Perseverance sol 110
227 and a minimum on sol 310, whereas by the Perseverance sol 414 (corresponding to
228 approximately L_s 212°) the atmospheric pressure is climbing higher than the first
229 maximum toward the annual maximum. When comparing Perseverance with concu-
230 rrent observations by the Curiosity Rover and the Insight lander as well as with the
231 historical Viking Landers data, we can see distinct differences in the amplitude of
232 the seasonal pressure variations that are due to different surface elevations.

233 The sol-averaged MEDA PS atmospheric pressure data together with the
234 hourly-averaged pressure depicted in Figure 4 is nicely showing the evolution of
235 the atmospheric pressure over first 414 Perseverance sols at the Jezero crater site.
236 In the beginning of the data set the pressure is going down during the Northern
237 spring and summer seasons and turning to an increasing leg during the late sum-
238 mer. The diurnal amplitude, shown approximately by the gray area in Figure 4,
239 shows a clear increase during periods with increased amounts of airborne dust start-
240 ing approximately from Perseverance sol 270 and staying high until sol 414 (when
241 our investigation period ends). There seems to be a direct relationship between the
242 range of diurnal pressure variation and the amount of airborne dust as has been
243 earlier discovered by, e.g., Zurek (1978, 1981); Paige and Ingersoll (1985).

244 The seasonal dependence of the Martian atmospheric pressure drives the at-
245 mosphere to the extent that about one third of the mass of the Martian atmosphere
246 is deposited on the polar caps during Northern and Southern winters and evapo-
247 rated back to the atmosphere during summertime. This results in the characteristic
248 atmospheric pressure pattern having two local maxima and minima during a Mar-
249 tian year, with the maxima occurring approximately at solar longitudes L_s 60°
250 and L_s 260°. This pattern can clearly be seen in Figure 5, which compares the sol-
251 averaged pressure of Perseverance with Curiosity Rover, Insight Lander, Viking
252 Landers and the Pathfinder mission. Table 1 gives the basic characteristics of each
253 mission.

254 Investigations of the seasonal pressure cycle together with observations from
255 other Martian landing missions enhance our understanding of the CO₂ cycle, the
256 annual heat balance of the polar caps and the global scale atmospheric circulation of
257 Mars (Paige & Ingersoll, 1985; Guo et al., 2009). Major drivers behind the seasonal
258 variation are solar radiation and surface and subsurface thermal properties (Wood
259 and Paige, 1992). Atmospheric dust loading and regional circulation will influence
260 short scale variations (Haberle et al., 1993; Hess et al., 1980). The annually aver-
261 aged atmospheric pressure is largely depending on the elevation of the site and hence
262 the atmospheric pressures are differing between observation sites (Hess et al., 1980;
263 Richardson & Newman, 2018).

264 In order to investigate the relative evolution of the pressure cycle at different
265 latitudes figures 5 (c) and 5 (d) show the differences in pressure between the Perse-
266 verance landing site and the other four landers, excluding Pathfinder. In figures 5
267 (c) and (d) a more negative pressure signifies a higher pressure compared to Perse-
268 verance. The results from MCD data shown in figure 5 (d) tracks in the evolution
269 of the results for the observational data shown in figure 5 (c). For Curiosity there

Table 1. Essential characteristics of seven Martian lander missions performing atmospheric observations. The elevations are based on MOLA data (Smith et al., 2001)

Vehicle	Lat (°N)	Lon (°E)	Elevation (km)	Climate Zone	Operational (years)	Platform Type
Viking lander 1	22	-48	-3.6	North sub-tropics	1976-82	Stationary
Viking lander 2	48	134	-4.4	North mid-latitudes	1976-80	Stationary
Mars Pathfinder	19	-34	-3.7	North sub-tropics	1997	Stationary
Phoenix	68	-126	-4.1	North polar regions	2008	Stationary
Curiosity	-4.6	137	-4.5	Equatorial regions	2012-	Mobile
InSight	4.5	136	-2.6	Equatorial regions	2020-	Stationary
Perseverance	18	77	-2.6	North sub-tropics	2021-	Mobile

270 are two sets of lines in figure 5 (c). These correspond to years 2 and 3 of the mission
 271 with year 3 being at a higher elevation which explain the difference in the mean
 272 pressure. There are a number of interesting dip or hump-like features over timescales
 273 of 100-200 sols in figure 5 (c) and (d) that need explaining.

274 The dips and humps in the season pressures in figure 5 (c) and (d) are most
 275 likely connected to latitude dependant processes that include the orographic, i.e.
 276 the large difference in elevation between the northern and southern hemisphere,
 277 and the dynamical effects on the pressure cycle (Hourdin et al., 1993). Regarding
 278 the orographic effect, during northern hemisphere winter a large mass of cool air is
 279 trapped in the low elevation of the northern hemisphere basin. In the winter a low
 280 atmospheric scale height traps a large portion of the atmosphere. The result is a
 281 higher winter maximum at higher latitudes in the northern hemisphere in winter.
 282 For example the heights of the winter and summer pressure peaks for Viking landers
 283 1 is much more symmetric than for Viking lander 2. We will not cover dynamical
 284 effect here, which is related to the winds, as it apparently has little influence at the
 285 equatorial and middle latitudes considered here. An explanation of the dynamical
 286 effect can be found in Hourdin et al. (1993).

287 The greatest dip seen is for the Viking lander 2 in 5 (d) which is at a lati-
 288 tude of 48°N. This results from the pressure observed by Viking lander 2 increasing
 289 more rapidly than the pressure observed by Perseverance most likely due to the oro-
 290 graphic effect. For the other landers the, except maybe for Curiosity, the pressure
 291 differences in figures 5 (c) and (d) are fairly level indicating the pressures at these
 292 landing site increase more or less at the same rate.

293 A shallow but distinct dip can be seen for Curiosity in figures 5 (c) and (d)
 294 over the spring-summer time period. A possible reason for a dip at this time of year

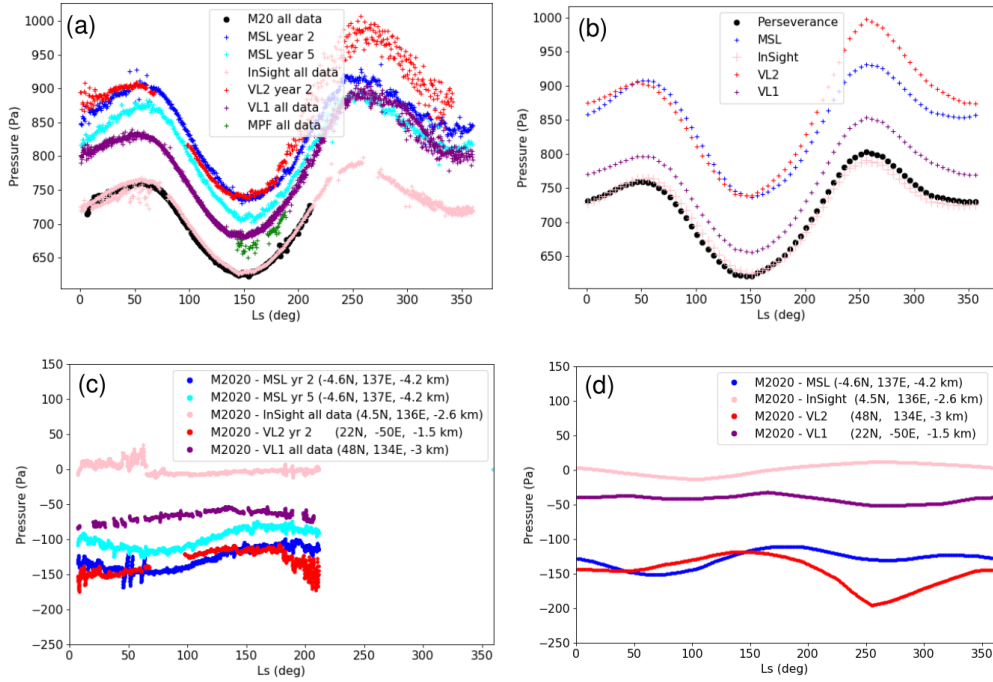


Figure 5. Comparisons of pressure between different lander missions. The top row shows the sol averaged observed pressure data, and the bottom row sol-averaged pressure data by different lander missions subtracted from Perseverance pressures. The left column shows results from the observations while on the right are the same results from the Mars Climate Database.

295 is that the cold air trapped in the northern hemisphere trapped during the winter
 296 is now being released as it is the summer. This lowers the pressure faster at the
 297 Perseverance landing site than at the Curiosity landing site, which is located near
 298 the equator in the southern hemisphere. This would result a relative increase in the
 299 pressure between Curiosity and Perseverance as seen in figure 5 (c) and (d). Both
 300 plots for Curiosity exhibit a dip around the summer solstice indicating that the pro-
 301 cess driving the evolution of the pressure, i.e. the dip, is not related to the change in
 302 elevation.

303 There are shallow dips and and troughs in the data for other landers in figures
 304 5 (c) and (d) but these are less obvious and probably cannot be interpreted with
 305 much certainty. For example there appears to be a small dip in the MCD data for
 306 InSight in figure 5 (d). This might be expected because InSight is located at a more
 307 southerly latitude than Perseverance with InSight being less sensitive to the ejection
 308 of summer time air from the northern basin than Perseverance. Interestingly this dip
 309 cannot be seen in Figure 5 (c) perhaps suggesting some other process or mechanism
 310 is masking the effect in the observations or limits with the model.

311 5 Diurnal atmospheric pressure and small scale atmospheric phe- 312 nomena

313 *In situ* pressure observations by several landed missions have shown that the
 314 Martian atmospheric surface pressure is composed of variations over several time
 315 scales and amplitudes. They include, *e.g.*, the overarching seasonal CO₂ cycle,
 316 regional-scale perturbations caused by planetary waves and thermal tides, including
 317 their interactions with topography, hydrostatic adjustment flows, and baroclinic and
 318 barotropic disturbances. Small scale eddies and disturbances, *e.g.* convective vortices
 319 are a usual cause of the shortest pressure variations of the order of a few tens of sec-
 320 onds (Harri et al., 2014, *e.g.*). If the vortices carry an optically distinguishable dust
 321 load they are called dust devils.

322 Thermal tides driven by solar irradiation cause distinct detectable diurnal pres-
 323 sure variations and are especially significant at low latitudes. In the Martian thin
 324 atmosphere the thermal tides - and hence the range of diurnal pressure variation
 325 - are much larger than in Earth's atmosphere due to the relatively stronger solar
 326 forcing at the surface (Zurek, 1982; Kieffer et al., 1992).

327 At the Jezero crater site measured by Perseverance rover the diurnal atmo-
 328 spheric pressure range seems to be approximately 20 Pa during the first 270 sols of
 329 the mission and thereafter during mission sols 270-414 extending to roughly 40 Pa.
 330 The wider range of diurnal pressure is likely due to increased amounts of airborne
 331 dust measured by Perseverance. Several earlier investigations have found the direct
 332 relationship between the amount of airborne dust and the range of diurnal pressure
 333 variation as shown by, *e.g.*, Zurek (1981, 1982); Guzewich et al. (2016).

334 The Perseverance *in situ* pressure observations show variations ranging from
 335 microscale to seasonal scale as has been observed by earlier *in situ* pressure mea-
 336 surements of Viking (Soffen, 1976; Soffen, 1977), Pathfinder (M. P. Golombek et
 337 al., 1999), Phoenix (Taylor et al., 2008) and Curiosity missions (Harri et al., 2014;
 338 Haberle et al., 2014). The advancing Martian season has a clear signature in the at-
 339 mospheric pressure as clearly manifested by Figure 6 depicting the diurnal pressure
 340 variation by data stacked in steps of 10 sols. It shows the gradual increase of the ob-
 341 served Perseverance pressure levels during the Northern spring until approximately
 342 sol 110, then gradual decrease bypassing the Northern midsummer (Ls 90) until sol
 343 320, and thereafter again showing increasing pressure until the last sol (414) of this
 344 investigation when the season advances further into the Northern fall. The data of

345 this investigation covers only 60 % of the Martian year, but this kind of seasonal
 346 dependence will be seen throughout the Martian year.

347 When inspecting the structure of diurnal pressure, 2-4 peaks appear in the
 348 data on each sol in Figure 6. A clear evolution of the peaks can be seen in the
 349 stacked diurnal pressure data. During Northern summer (Figure 6, second row
 350 from top) diurnal pressure exhibits two distinct and regular peaks, one in the morn-
 351 ing around 6-7 AM and the other one around 8-9 PM LTST. During the Northern
 352 spring (Figure 6, top row) and fall (Figure 6, lowest rows) this summertime regular
 353 pattern is broken into more like four separate peaks whose amplitudes vary along
 354 with advancing season.

355 It seems that during springtime - at the start of the mission, Perseverance sols
 356 0-150 - smaller peaks are superimposed on the larger peaks. These smaller peaks dis-
 357 appear between about sols 150 and 250 (Northern summertime) and return around
 358 sol 300 in early Northern fall. The wintertime has not yet come during the first 414
 359 Perseverance sols. The features in the plots give clues on the behaviour of regional
 360 atmospheric dynamics and circulation patterns in the Martian atmosphere (Read &
 361 Lewis, 2004, e.g.).

362 The largely repeatable two-peak shape of the daily surface pressure profile
 363 especially during the Northern summertime (Figure 6) is likely due to the strong
 364 semi-diurnal thermal tidal component as indicated in Figure 7. Abundant amount of
 365 airborne dust is one cause responsible for amplified semi-diurnal tidal component as
 366 shown by, e.g., (Zurek, 1981; Newman et al., 2021). Similar two-peak structure was
 367 also discovered during Pathfinder mission Schofield et al. (1997).

368 The harmonic components – principal components - of daily pressure variations
 369 sheds light on our understanding on the atmospheric phenomena behind the com-
 370 plex structure of daily pressure cycle. The principal components of the atmospheric
 371 diurnal pressure variation can be revealed by decomposing the pressure observations
 372 through Fourier transformation. The estimated diurnal, semi-, ter- and quad-diurnal
 373 amplitudes are represented by the first four components of the resulting series repre-
 374 sentation, respectively, as shown in Figure 7 together with the Perseverance optical
 375 thickness observations.

376 The Fourier transformations shown in Figure 7 were calculated using a fast
 377 Fourier transform (FFT) scheme. The input data series was created by generating
 378 hourly bins of observations from a window of three sols to get at least one observa-
 379 tion per hour. In case of multiple observations per hour the bin value was achieved
 380 by averaging. The middle sol of the three-sol window was the one that was assigned
 381 the calculated amplitudes and phases. When using this procedure it was assumed
 382 that the three consecutive sols were sufficiently similar for calculating the principal
 383 components. The analysis was performed by sliding the three-sol window over the
 384 first 414 sols of Perseverance observations.

385 The principal components of the Perseverance diurnal pressure variation seem
 386 to be smaller than those measured by the Curiosity rover at Gale crater where tidal
 387 forcing is stronger due to the location close to the equator and also due to the fact
 388 that, at Curiosity’s longitude sector, eastward and westward modes are expected to
 389 interact constructively (Wilson and Hamilton, 1996; Haberle et al., 2013; Harri et
 390 al., 2014).

391 In the light of the strong semi-diurnal component shown in Figure 7 during the
 392 Northern summer (sols 150-250), the prevailing stable 2-peak diurnal pressure cycle
 393 may be due to the strong summertime tidal forcing by relatively high amount of re-
 394 gional airborne dust creating a strong and stable semidiurnal component (Figure 7,
 395 top panel). This situation resembles that in the terrestrial tropics, where diurnal

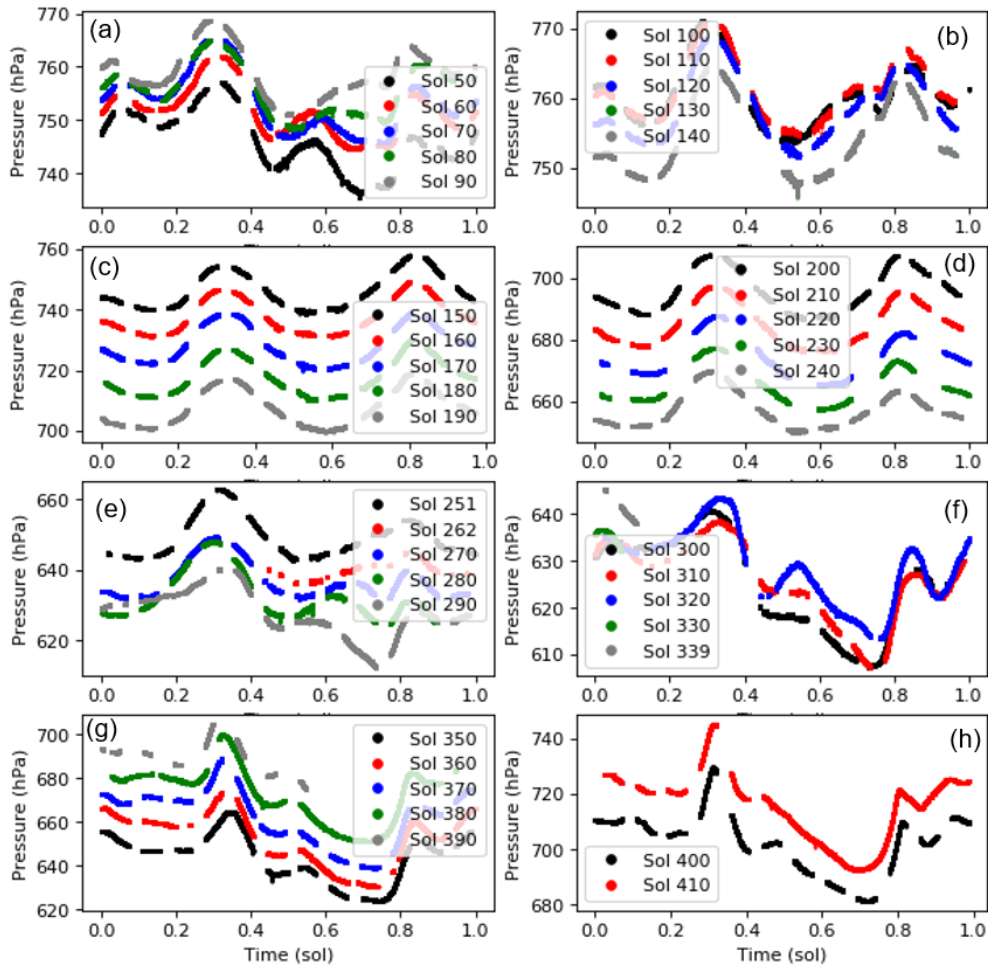


Figure 6. Evolution of diurnal pressure variation in steps of 10 sols covering the first 414 Perseverance sols during the advancing season. Each figure shows data averaged over five sols centered on the sol number shown, except the last on the bottom right (pane h).

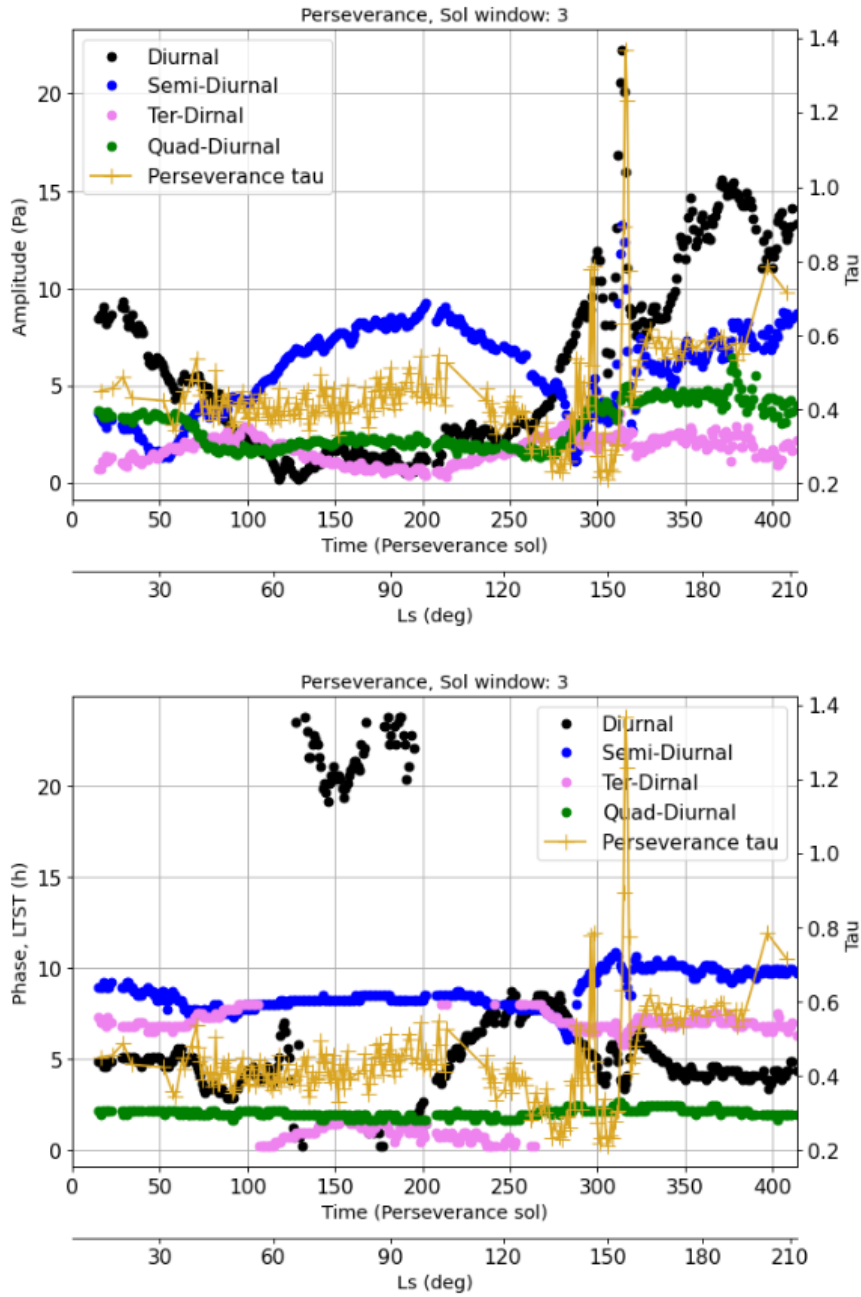


Figure 7. The amplitude and phase of the first four harmonic components of diurnal pressure calculated using FFT for all Perseverance sols. A running averaging window of three sols was used in the calculations. The amplitudes (top pane) and phases (lower pane) are illustrated in different colors (left axis). On the amplitude plot also the optical thickness observed by Perseverance is also shown (right axis).

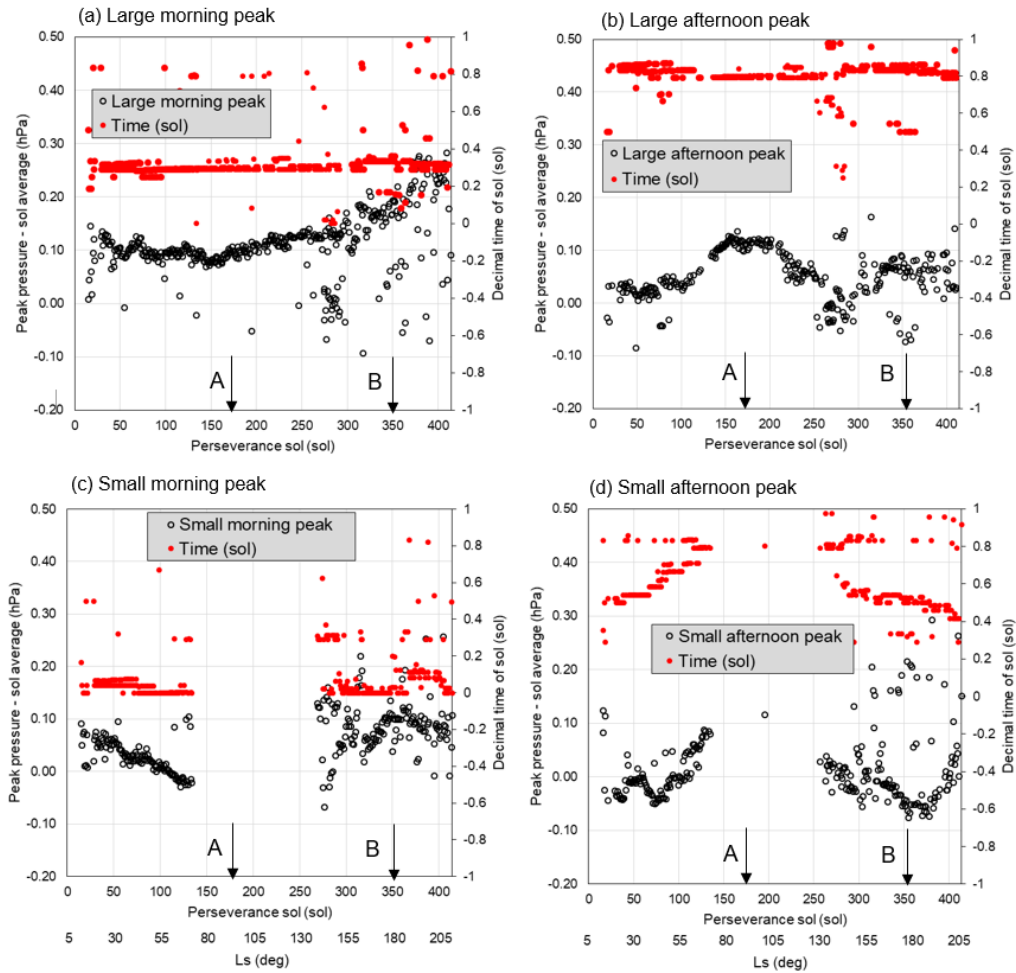


Figure 8. Black circles show the peak pressure minus sol averaged pressure. The time of occurrence of the peaks is also shown in red. The time has an uncertainty on it of plus or minus half an hour. The scatter in the points arises from relatively small fluctuations in flat regions of the data, *e.g.* in the dips between the peaks. The letters 'A' and 'B' point to midsummer (L_s 90°) and fall L_s 180°, respectively.

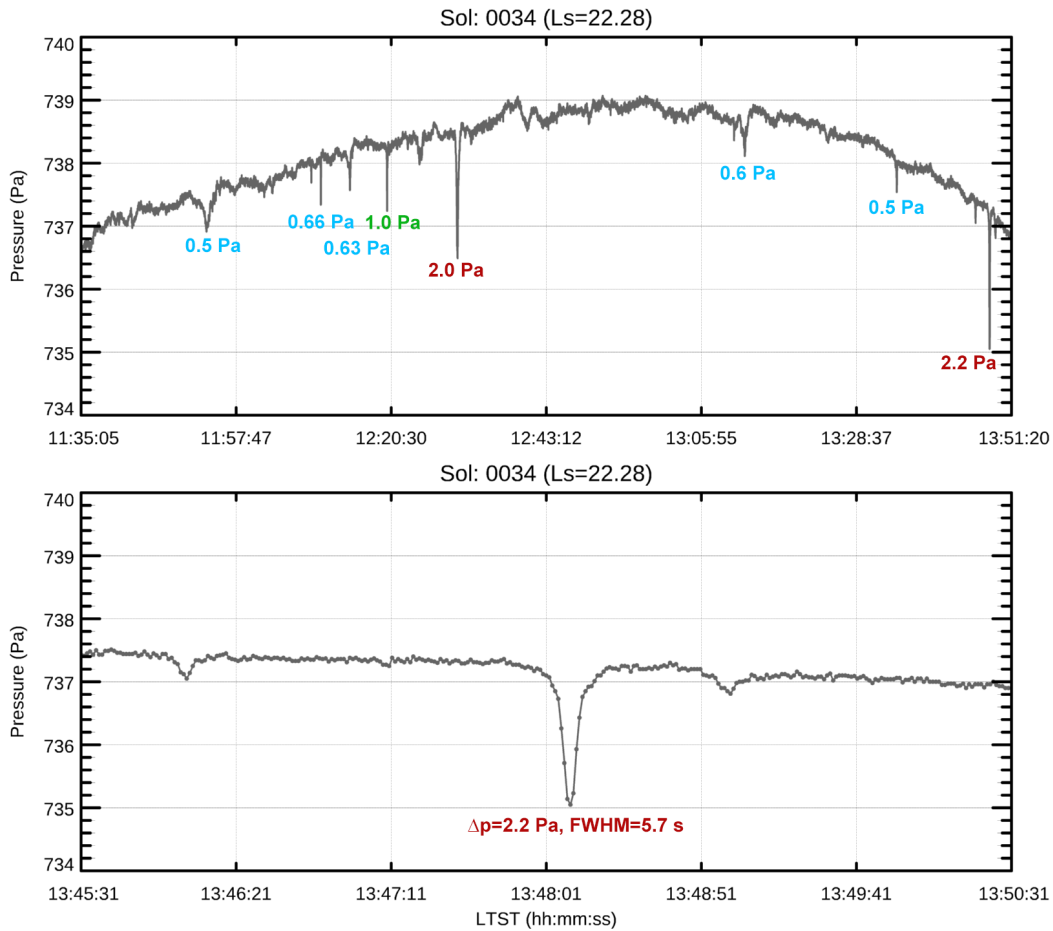


Figure 9. An example of vortex activity detected in pressure data over a 1.5 hour period around noon during the Perseverance mission sol 34. The upper pane displays vortex activity that can be seen as downward spikes in pressure with the depth of some spikes indicated. The lower pane zooms in on the deepest spike (2.2 Pa) to show a more detailed spike structure indicating also the full width at half maximum (FWHM) of the spike.

396 pressure has two distinct peaks, too – one in the morning and one in the evening.
 397 In the terrestrial tropics this is due to high-altitude ozone, whereas in northern late
 398 spring and early summer on Mars this may be due to the ever-present airborne dust
 399 getting heated by solar irradiation (Read and Lewis, 2001).

400 The semidiurnal tidal component at Jezero crater seems to be strong during
 401 Perseverance’s Northern summer. This may be due to the fact that regional atmo-
 402 spheric dust load is relatively high at that time, which would amplify the semidi-
 403 urnal component - assisted by the strong solar forcing at the Northern summer.
 404 Optical depth maps retrieved from the Mars Climate Database, based on data sets
 405 generated by Montabone et al. (2015), seem to support our inference. The maps
 406 from the MCD suggest that during the summer Perseverance is on the western
 407 edge of a patch of elevated optical depth that stretches over several 10s of degrees
 408 of longitude to the west. Later on in the year the optical depth at the latitude of
 409 Perseverance is more homogeneous.

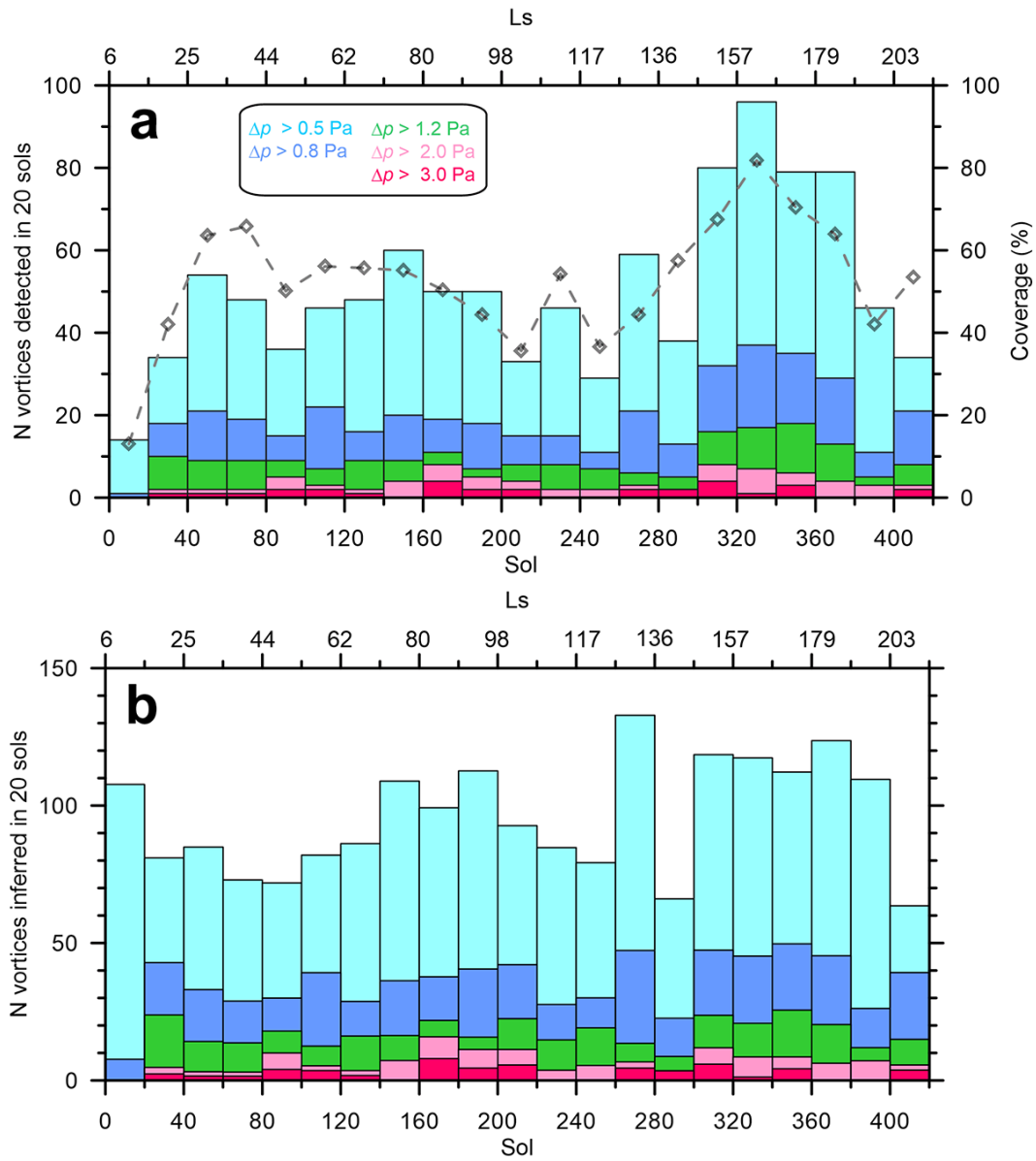


Figure 10. Assessment of the number of vortices by Perceverance through atmospheric pressure drops as a function of sol. (a) Number of vortices actually detected in intervals of 20 sols (left axis). The rhombs show the coverage of MEDA pressure data in each time interval (right axis). (b) Number of vortices that would have been detected if MEDA data would have been measured continuously. In both panes the intensity of the pressure drops is indicated by color coding as explained in the legend.

410 The seasonal evolution of diurnal pressure and its pattern of variation is shown
 411 in Figure 6. We found that during the Northern summertime a fairly stable pattern
 412 of two peaks was prevailing in diurnal pressure variation, but that was broken into
 413 four peaks during the spring and fall. Now, we can study further the evolution of
 414 the daily pressure pattern by analyzing the peaks and their evolution with the ad-
 415 vancing season (Figure 8). This is done by subtracting the average pressure of the
 416 sol of interest from maximum pressure to get the peak amplitude and also noting the
 417 local time of occurrence.

418 Figure 8 shows the peak pressures relative to the daily-averaged sol pressure
 419 and the time that the peaks occur. As can be seen in Figures 6 and 8 there is one
 420 large peak both in the morning and in the afternoon that persist in the daily pres-
 421 sure data. These are clearly illustrated in the top row of Figure 8. The time these
 422 peaks occur remains steady throughout sols 50 to 400 in the data. Their magni-
 423 tude varies with the large morning peak increasing after about sol 150. The large
 424 afternoon peak reaches a maximum around sol 150.

425 Figure 6 shows small morning and afternoon peaks prevailing during North-
 426 ern springtime and fall. They are also depicted in Figure 8, where it can be seen
 427 (bottom row) that the small morning peak occurs at the same time each sol but the
 428 magnitude decreases until about sol 140 and then the peaks disappear. They reap-
 429 pear around sol 270 but appear to fluctuate in magnitude before settling down to
 430 a near constant value around sol 360. In Figure 8 (lower right) the small afternoon
 431 peaks appear to increase in magnitude before disappearing around sol 140. They
 432 then reappear around sol 260 and decrease in magnitude with the advancing sols.

433 These interesting morning and afternoon peak variations illustrated by Fig-
 434 ures 6 and 8 could be a manifestation of local circulation phenomena causing pres-
 435 sure variation, which is then superposed with the strong semidiurnal pressure mode.
 436 During the Northern summer the semi-diurnal thermal tide (as shown by the semi-
 437 diurnal pressure variation) is at its strongest, which creates a stable diurnal pressure
 438 variation with one distinct large peak in the morning and another one in the af-
 439 ternoon. During the Northern spring and fall the semidiurnal mode of the thermal
 440 tide is weaker than in summer. Hence the stable situation is broken resulting in the
 441 creation of two additional small peaks, one preceding the large morning peak and
 442 another preceding the large afternoon peak.

443 This kind of pressure peak structure riding on top of the diurnal pressure
 444 variation is possibly caused by local effects due to the more complex topography
 445 of Jezero crater as compared, *e.g.*, to the topographically more simple and flat re-
 446 gion of the Pathfinder and Viking Lander sites (Soffen, 1976; Schofield et al., 1997),
 447 where such peaks are not so clearly visible. On the other hand, at the Curiosity
 448 rover site additional peaks are also seen in the diurnal pressure variation, which is
 449 likely due to the fact that Gale crater is also a topographically complex site (Harri
 450 et al., 2014; Haberle et al., 2014). Variations in the thermal tide could also intro-
 451 duce multiple oscillations into the observed surface pressure. Schofield et al. (1997)
 452 suggest interference effects between the westward tide and the eastern travelling to-
 453 pographically induced Kelvin mode could produce surface pressure observations with
 454 two minima and two maxima per sol.

455 A highly interesting atmospheric phenomenon regularly observed in pressure
 456 data are convective vortices - called dust devils when raising surface dust in the
 457 atmosphere (Zurek, 1982; Ferri et al., 2003, *e.g.*). These rotating small scale atmo-
 458 spheric phenomena are investigated in this journal issue by (Hueso et al., 2023) us-
 459 ing Perseverance pressure observations. Vortices appear as pressure drops in MEDA
 460 data, some times in bursts of activity as displayed by Figure 9 and 10 based on the
 461 investigations by Hueso et al. (2023). These pressure drops are most likely caused

462 by passages of thermal vortices. Some of these events can be identified as dust devils
 463 when observing with additional MEDA radiative sensors able to infer the presence
 464 of dust, and by other instruments onboard Perseverance such as rover cameras. In
 465 the context of the Aeolian environment of Jezero, thermal vortices were discussed
 466 by Newman et al. (2022). These studies provide the overall abundance of vortices
 467 at Jezero, their daily cycle of activity, which peaks roughly at local noon, with some
 468 seasonal variation in the transition from summer to fall, the frequency of vortices
 469 that carry dust and are therefore dust devils, and establish the link between vortex
 470 activity and the thermal gradient of the near surface atmosphere.

471 An interesting aspect of vortex activity at Jezero revealed originally by the
 472 work of Hueso et al. (2023)) is the nearly constant activity with little seasonal varia-
 473 tion during the period of observation of this investigation. This is demonstrated by
 474 Figure 10 showing the statistics of detected and estimated amount of vortices during
 475 the period of the first 414 Perseverance sols. This allows us to estimate (Figure 10)
 476 that about 100 thermal vortices with pressure drops exceeding 0.5 Pa during a 20
 477 sol period are dwelling in the Perseverance neighbourhood throughout the first 414
 478 Perseverance sols. Thus the vortex activity at Jezero seems to be nearly constant
 479 through the first 414 Perseverance sols. Apparently solar forcing varying consider-
 480 ably from springtime to fall has not significantly affected the generation of vortices.
 481 It is interesting to see whether this pattern will hold through the upcoming North-
 482 ern wintertime with decreasing thermal forcing.

483 Martian atmospheric small scale turbulence and dynamics can be investigated
 484 using Perseverance observations accompanied by additional Perseverance measure-
 485 ments. These phenomena are studied in an accompanying paper in this journal issue
 486 by Sánchez-Lavega et al. (2023).

487 **6 Perseverance diurnal pressure compared with other landing sites** 488 **and modeling results**

489 Atmospheric diurnal pressure variation is affected by *e.g.* the strength of ther-
 490 mal tide, regional and local geography and amount of airborne dust and hence some
 491 local atmospheric phenomena can be partially explained by studying diurnal pres-
 492 sure variation (Zurek, 1982; Zurek et al., 1992b; Haberle et al., 2014; Harri et al.,
 493 2014, *e.g.*). The diurnal pressure amplitude – minimum to maximum range – as a
 494 function of solar longitude for both Perseverance and Curiosity rovers is depicted
 495 in Figure 11 including the measured optical depth. Additionally results by regional
 496 models MWRP (squares) and MRAMS (plus-signs), as well as values by Mars Cli-
 497 mate Database (diamonds) are shown. Furthermore, an uncertainty corridor of two
 498 standard deviations is drawn on the pressure amplitude by smoothing over a few
 499 sols. The standard deviation of the diurnal pressure range is calculated over 10 sols
 500 and it is then drawn on both sides of the curve. Thus the width of the uncertainty
 501 shown is thus twice the standard deviation.

502 The diurnal pressure variation exhibits a clear amplitude increase with the
 503 increasing amount of the atmospheric dust, which was reported by Curiosity pres-
 504 sure observations (Haberle et al., 2013; Harri et al., 2014). This phenomenon has
 505 been discovered also earlier by, *e.g.* Zurek (1978, 1982); Tillman (1988); Kahre and
 506 Haberle (2010). Actually, this is considered as a manifestation of how the Martian
 507 atmospheric conditions are intertwined with the airborne dust to such extent that
 508 atmospheric diurnal pressure observations could even be used to infer the amount of
 509 dust afloat *e.g.* (Zurek, 1981; Guzewich et al., 2016).

510 Figure 11 shows that the observed daily amplitudes in pressure are similar to
 511 those predicted by two atmospheric models that cover Jezero crater at km scale

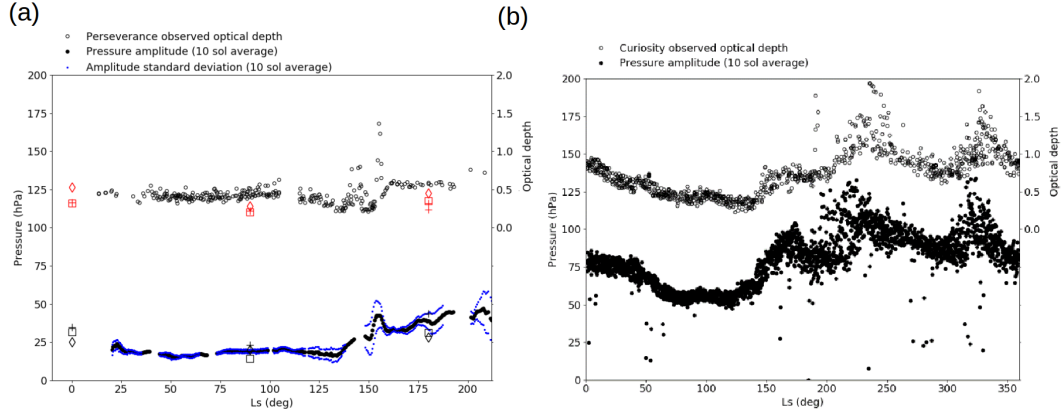


Figure 11. Diurnal pressure amplitude – minimum to maximum range – as a function of solar longitude (black dots, left axis) and the optical depth (small black spheres, right axis). The plots in (a) includes Perseverance pressure (MEDA PS) and optical thickness (M2020 Mastcam-Z) data during the first 414 Perseverance sols and in (b) all Curiosity pressure (REMS-P) and optical thickness (MSL Mastcam) data until Perseverance mission time. The depicted diurnal pressure range is a 10-sol moving average in both plots. The Perseverance plot also includes a 2-sigma belt around the diurnal pressure with the standard deviation (sigma) calculated from the 10 sols for each average point. Additionally results by regional models MWRF (squares) and MRAMS (plus-signs), as well as values by Mars Climate Database (diamonds) are shown.

512 resolution (MRAMS and MarsWRF). The amplitude predicted by MRAMS is usu-
 513 ally slightly higher and MarsWRF slightly lower, for the Ls with data available. The
 514 models use TES optical depth zonally averaged over previous non dust storm years
 515 (Pla-Garcia et al., 2020) (Newman et al., 2021). As to the MCD values for the loca-
 516 tion of Perseverance (18°N, 77°E) the optical depth used in these models is similar
 517 to those observed by Perseverance. Note that the pressure amplitude in the MCD,
 518 which has a resolution of order several hundred km, is also similar to that observed
 519 by Perseverance.

520 It is interesting to compare the average amplitude of diurnal pressure varia-
 521 tion – minimum to maximum value – at different locations and for varying Martian
 522 altitudes and terrain. The Martian atmospheric pressure has some interannual varia-
 523 tion, but it appears to be sufficiently small to the extent that the atmospheric pres-
 524 sure at each landing site seems to be behaving largely in a similar fashion from year
 525 to year as shown by, *e.g.*, Tillman (1988); Tillman et al. (1994). This interannual
 526 similarity justifies qualitative and also somewhat quantitative comparison of pres-
 527 sure by different landing missions even if they are not observed at the same time,
 528 but rather in different Martian years. This applies especially to diurnal pressure
 529 variation that is being largely driven by thermal tide, local geography and regional
 530 atmospheric flows.

531 Figure 12 depicts the daily pressure amplitude during the first 414 sols of the
 532 Perseverance mission with concurrently observed daily pressure amplitudes of the In-
 533 sight and Curiosity missions, as well as that of historical Viking Landers, Pathfinder
 534 and Phoenix mission data at matching solar longitudes. Basic characteristics of
 535 those seven Martian missions are shown in Table 1 including the climate zones and
 536 geographical locations (also in Figure 1) of those missions.

537 It can be readily seen in Figure 12 that the daily pressure amplitude of Per-
 538 severance, Viking Lander 1 and Pathfinder are quite similar, which is likely caused
 539 by the fact that they are at similar latitudes and experience similar thermal tides.
 540 The tides also have a distinct pattern in longitude too, though, due to interference
 541 by the large-scale topography although this does not seem to be a factor here. A
 542 regional dust storm like in the case of Viking Lander 1 starting on around L_s 200°
 543 increases the amplitude. In the case of Pathfinder the amplitude variation increases
 544 considerably as a function of the Martian season (Schofield et al., 1997). The diurnal
 545 pressure amplitude seems to be highest at the Curiosity and Insight landing areas,
 546 which are located close to the equator and hence have the strongest thermal tides.
 547 On the other hand, Phoenix observations have the lowest diurnal pressure amplitude
 548 as expected due to the weaker thermal tide occurring at such high latitudes.

549 Basic characteristics of those seven Martian missions are shown in Table 1
 550 including the climate zones and geographical locations (also in Figure 1) of those
 551 missions. It is to be noted that similarities on some of those characteristics allow
 552 interesting considerations to be made. Insight and Perseverance have a very sim-
 553 ilar altitude above the Martian geoid, which allows for direct comparison of the
 554 sol-averaged pressure data including the pressure variation with advancing Martian
 555 season. This is the most direct possibility for comparisons. As to the longitudinal
 556 location, Perseverance seems to be relatively isolated from the other landed missions.
 557 When inspecting the latitudinal location, Perseverance shares the same climate zone
 558 – North subtropics – with the Pathfinder and Viking 1 landers and is similarly able
 559 to feel the additional effects of baroclinic disturbances through the mesoscale small
 560 pressure variations that these disturbances cause at the surface. The same applies
 561 also to the traveling low- and high-pressure systems – typical both on Mars and
 562 the Earth - causing pressure variations in a 2–5 sols time range especially in the
 563 wintertime subtropics and low midlatitudes (James et al., 1992).

564 The shape of diurnal pressure variation at different Martian landing sites in
 565 four periods evenly separated over the first 414 Perseverance sols are shown in Fig-
 566 ure 13. In each case, two sols of data are shown figure 13 (top left) shows clearly
 567 that the diurnal pressure amplitude observed by Curiosity in Gale crater is larger by
 568 a factor of 2-3 than for Perseverance in Jezero crater. The diurnal pressure ampli-
 569 tude observed by some other landing missions (Figure 13, top right) – Pathfinder,
 570 Viking Landers, Insight - is also smaller than what Curiosity has observed. The
 571 large amplitude of pressures observed by Curiosity has been shown by using atmo-
 572 spheric models to arise from the influence of a daily cycle of heating on the large
 573 slopes of Gale crater, such that warming of air causes mass to flow out of the crater
 574 in order to maintain hydrostatic balance along the slopes (Richardson and New-
 575 man, 2018). Perseverance observations indicate that the diurnal pressure range at
 576 the Jezero crater is smaller by a factor of 2-3, somewhat smaller amplitude than
 577 measured by Insight, about the same amplitude than calculated from historical ob-
 578 servations of Viking lander 1 and 2 and, however, somewhat larger than diurnal
 579 pressure range measured by the Phoenix mission.

580 In the two lower rows of Figure 13 (panes c-f), approximately two sols for each
 581 lander at four solar longitude values marked in panes a-b are shown. Perseverance
 582 can be seen to have a similar mean pressure to InSight. This is likely due the similar
 583 elevations of around -2.6 km. The diurnal pressure patterns are similar in amplitude
 584 but slightly out of phase between Perseverance and InSight, most likely due to the
 585 59° difference in longitude, i.e. the thermal tide will pass over Insight and then over
 586 Perseverance four hours later. Also note that the diurnal patterns for Curiosity and
 587 InSight, separated by only one degree of longitude, are similar except that Curiosity
 588 has a greater diurnal amplitude.

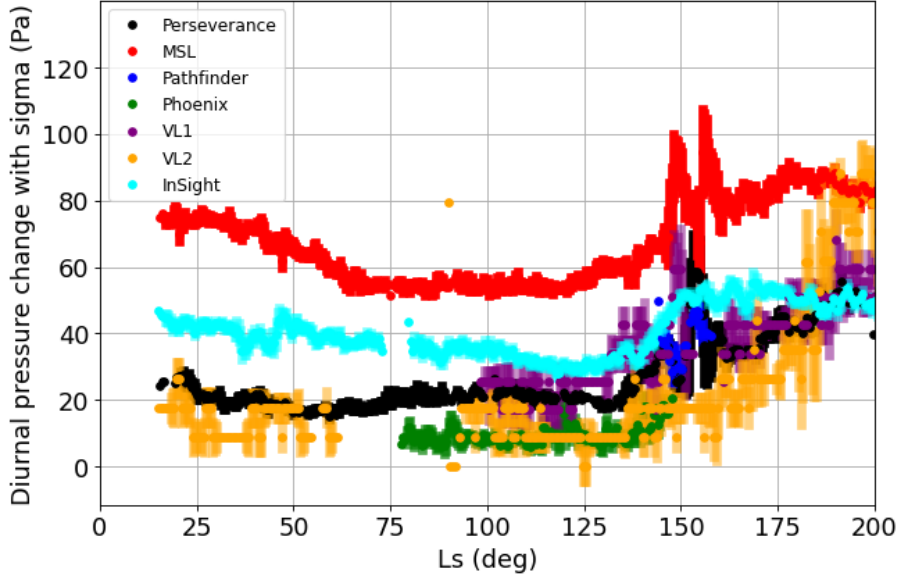


Figure 12. Diurnal pressure amplitude – minimum to maximum value – during the first 414 sols of the Perseverance mission with concurrently observed diurnal pressure amplitude of InSight and Curiosity missions, as well as that of historical Viking Landers, Pathfinder and Phoenix mission data on matching solar longitude range. Each diurnal pressure point is a moving 3-sol central average. The thickness of the curves represent the value of 2 standard deviations calculated over seven sols around each average diurnal pressure point.

589 At the Viking lander 2 site the daily pressure amplitude approaches similar
 590 levels to those observed by Curiosity only in the second half of the year, i.e. in the
 591 winter, as can be seen in figure 13 (b). The diurnal pressure amplitudes for the
 592 landers at high latitudes, i.e. Phoenix and Viking lander 2, during the northern
 593 hemisphere summer are small because of the weak thermal tide (Zhao et al., 2015).
 594 Curiosity and InSight latitudes (Table 1) are close to the equator and both have
 595 consistent daily pressures amplitudes throughout the year suggesting little variation
 596 in the thermal tide conditions at these latitudes.

597 Regional atmospheric modeling efforts are needed to expand the value of the
 598 *in situ* observations. This was done by running MarsWRF and MRAM models (Pla-
 599 Garcia et al., 2021) at the Perseverance site on solar longitude values of L_s 270°,
 600 90°, 180° and 270°. Figure 14 illustrates these results together with *in situ* Persever-
 601 ance observations at L_s 0°, 90°, 180° as well as data points acquired from the Mars
 602 Climate Database MCD (LMD-Jussieu, 2021).

603 MarsWRF and MRAMS simulate Jezero crater at high resolution. Mar-
 604 sWRF is a mesoscale nest embedded inside a global model model and MRAMS is
 605 a mesoscale model. Overall, MarsWRF and MRAMS as well as the lower-resolution
 606 MCD do fairly well compared to the actual *in situ* pressure observations. MarsWRF
 607 seems to reproduce the dip at 1700 better than MRAMS in Figure 14. MarsWRF
 608 reproduces the main features quite well except the small peaks at noon in the North-
 609 ern springtime (L_s 0°, Figure 14a) and fall (L_s 180°, Figure 14c) where it generates
 610 a shoulder-like feature instead. The average pressure in Figure 14a for MarsWRF
 611 is generally good but in the Northern summertime (L_s 90°, Figure 14b) and fall
 612 (Figure 14c) the average pressure is too low. The height of the peaks in Figure 14b

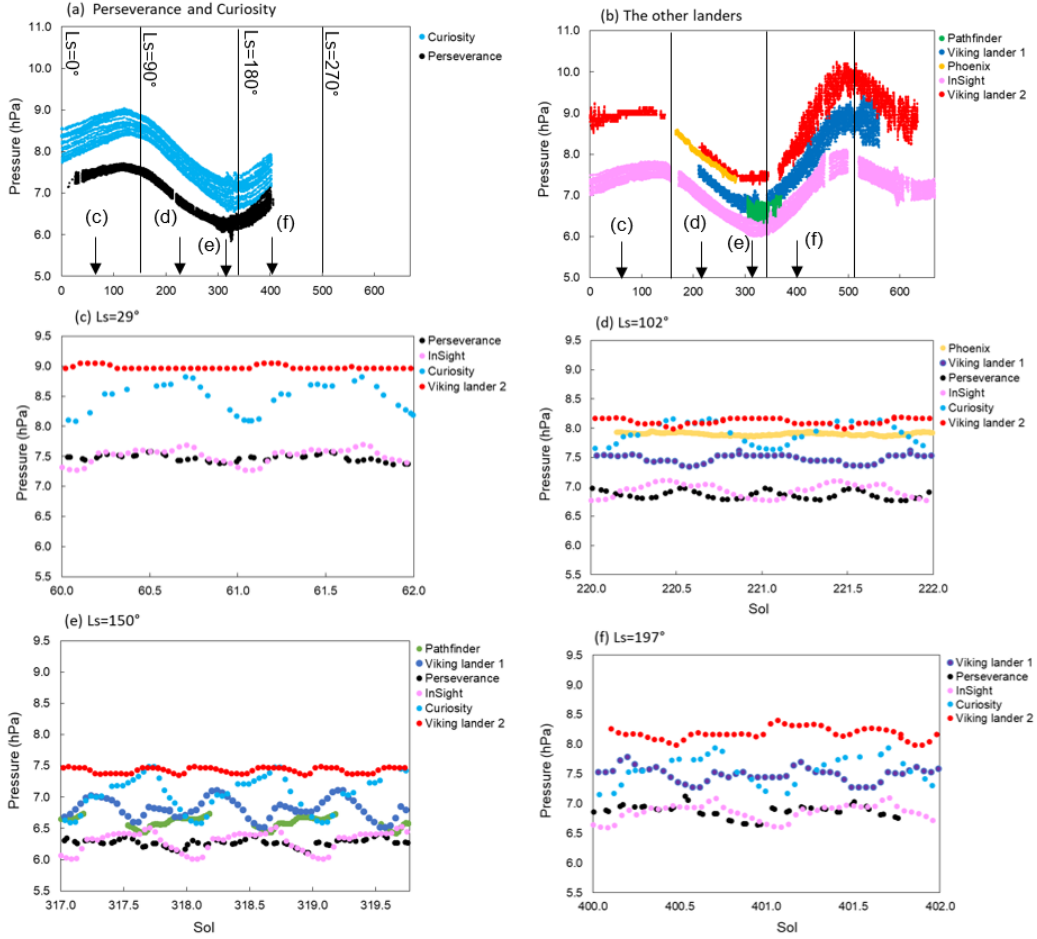


Figure 13. Diurnal pressure range of the Perseverance Rover compared over seasons with the diurnal pressure ranges observed by the Curiosity Rover, Insight Lander, Viking Lander 2 and Pathfinder (top row). Detailed diurnal pressure variation over 2-sol periods on these five surface missions is depicted at four solar longitudes evenly covering the first 414 sols of Perseverance operations. The lander data is plotted against the yearly sol, i.e. midnight on sol 1 corresponds to $L_s=0^\circ$ at the prime meridian, with midnight offset at each landing site depending on their longitude. The 2-sol periods were chosen in (c) to (f) over periods that avoided gaps in the lander data.

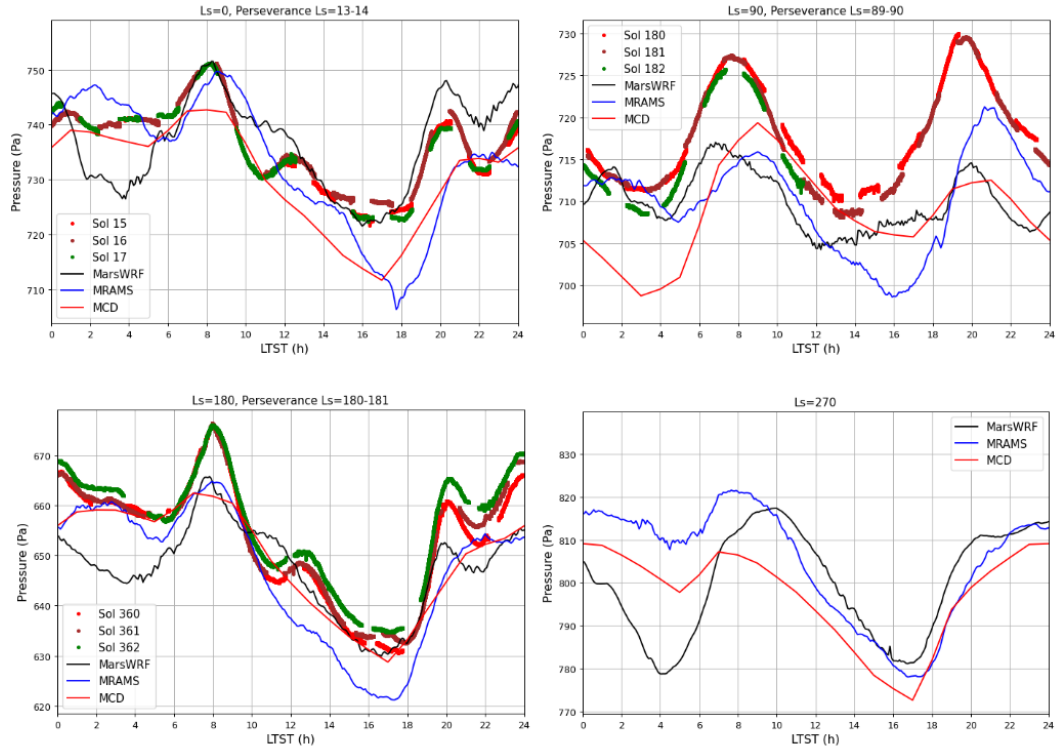


Figure 14. Diurnal pressure variation modeled by atmospheric models that simulate Jezero at km grid spacing MarsWRF, MRAMS and also the same data points from Mars Climate Database at solar longitude L_s 0° , 90° , 180° and 270° , which are depicted in panes a) to d). Around the solar longitude 0, 90 and 180 Perseverance pressure observations from three sols are added (Perseverance has no data as yet at L_s 270°).

613 are too low in the MarsWRF data. MCD is roughly producing in the average similar
614 results to Mars WRF and MRAMS.

615 MRAMS matches the average pressure level quite well in Figure 14a if it was
616 not for the big dip at 1700. It is not clear if it reproduces the peaks at 2200 and
617 midnight. The occurrence of the peaks in the MRAMS data seems to be delayed
618 by about 2 hours. Like MarsWRF MRAM does not reproduce the small peak at
619 noon. MRAMS reproduces the height of the two big peaks in Figure 14b but they
620 are on average too low. The timing of the peaks seems to be delayed by about 2
621 hours in Figure 14b. Overall, it seems to be the case that state-of-the-art regional
622 atmospheric models succeed fairly well in producing diurnal pressure variation at
623 the Jezero crater region. Then, understandably, reproducing through modeling the
624 small peaks in diurnal pressure variation caused largely by the local geography and
625 atmospheric flow conditions proves to be challenging.

626 The distinct oscillations in the observed surface pressure are expected to be
627 primarily due to the thermal tides and their interactions with the Martian topogra-
628 phy, e.g. Wilson and Hamilton (1996). Oscillations in the pressure could also include
629 contributions of the local crater circulations that are especially important for deep
630 craters like Gale crater (Tyler and Barnes, 2015; Wilson, 2017). In addition hydro-
631 static adjustment has been shown to be important in amplification of the amplitude
632 of the diurnal pressure variation (Richardson and Newman, 2018).

633 This complex structure in the pressure signal was anticipated by Pla-Garcia
634 et al. (2020). This is demonstrated in a distinct fashion in figure 14. A more com-
635 prehensive modeling study is needed, but the Perseverance pressure observations
636 support the initial regional atmospheric modeling results at the Perseverance site
637 made with the Mars WRF and MRAMS models as well as the data provided by
638 MCD.

639 Jezero crater does not seem to have a similarly strong amplification from hy-
640 drostatic adjustment as is the case at the Gale crater based on the observations by
641 the Curiosity rover (Harri et al., 2014; Newman et al., 2021). A plausible reason for
642 this is the fact that compared to the Gale crater, the Jezero crater is shallow and
643 wide resulting in relatively weaker amplification effect on the diurnal pressure vari-
644 ation amplitude. In addition the thermal tide at the Gale crater is stronger at most
645 times of year than at Jezero crater because it is closer to the subsolar point for most
646 of the year.

647 Combining the atmospheric regional modeling with *in situ* pressure observa-
648 tions proves to be highly useful – it adds the value of the observations by expanding
649 their effect beyond the actual point of observation and sheds more light on the phys-
650 ical and meteorological processes behind the Martian atmospheric phenomena. The
651 physics and implementation of the models themselves can also be modified to better
652 address the actual atmosphere.

653 **7 Summary and discussion**

654 The Mars2020 Perseverance Rover landed successfully onto the Martian sur-
655 face on the Jezero Crater floor (18°N, 77°E) at the Martian solar longitude L_s 5° in
656 February 2021. Since then it has produced highly valuable environmental measure-
657 ments with a versatile scientific payload including a suite of environmental sensors
658 MEDA (Mars Environmental Dynamics Analyzer). One of the MEDA sensor sys-
659 tems is MEDA PS pressure device weighing 40 grams.

660 The Martian atmospheric pressure observations by MEDA PS have proved to
661 be of excellent quality fulfilling expectations with the estimated overall uncertainty

662 being equal or better than 3.5 Pa and the resolution about 0.13 Pa. The system
 663 resources required by the whole MEDA PS package are dimensions being $62 \times 50 \times 17$
 664 mm, mass 40g and power consumption less than 15 mW.

665 This paper presents initial results of the first 414 sols of Martian atmospheric
 666 surface pressure observations by the MEDA PS device whose performance was found
 667 to fulfill the specification. Observations controlled by the Perseverance resources
 668 allocation schedule cover approximately 50 – 70 % of the Perseverance operational
 669 time.

670 The atmospheric pressure measurement device (MEDA PS) is based on the
 671 silicon-micro-machined pressure sensor head (Barocap®) and transducer technology
 672 developed by Vaisala Inc. The Barocap® version used by MEDA PS is optimized
 673 for the Martian near-surface atmospheric pressure. The transducer electronics and
 674 required electromagnetic shielding and mechanical support structures were developed
 675 by Finnish Meteorological Institute (FMI).

676 The MEDA PS pressure device is making measurements continuously with 1
 677 Hz frequency in average for every other hour according to the operational schedule
 678 by the Perseverance Rover. That enables us to generate data sets with averaged
 679 pressure measurements approximately at 1-hour intervals, as well as data sets with
 680 pressure observations at 1 second intervals for one or a few hours in a row for short
 681 time scale studies. In this work we use data sets with 1-hour intervals. The 1-hour
 682 data sets are not complete but they do have some gaps due to scheduling of Perse-
 683 verance and MEDA operations. However, the available data coverage allows good
 684 characterisation of both the diurnal and seasonal variations in the pressure.

685 The seasonal-to-annual time scales the CO₂ condensation-sublimation cycle
 686 of the Martian atmosphere is nicely demonstrated at the Jezero crater site by the
 687 Perseverance Rover measurements. The observed sol-averaged atmospheric pres-
 688 sure during the 414 first Perseverance sols from the landing time at early Northern
 689 springtime to Northern fall follow an anticipated pattern of total pressure varia-
 690 tion in the course of the advancing season. The data has the first maximum in late
 691 spring roughly on the Perseverance sol 110 and minimum on sol 310, whereas by
 692 the Perseverance sol 414 corresponding to approximately L_s 212° the atmospheric
 693 pressure is climbing higher than the first maximum toward the seasonal maximum.
 694 When comparing Perseverance with concurrent observations by the Curiosity Rover
 695 and the Insight lander as well as with the historical Viking Landers data, we can see
 696 distinct differences with the amplitude of the seasonal pressure variation that are
 697 due to different surface elevations.

698 When comparing pressure observations of the seven Martian landing missions
 699 on different locations on Mars the first part of seasonal atmospheric pressure cycle
 700 measured by Perseverance seems to follow the seasonal increase and decrease in the
 701 atmospheric pressure as expected. The visible bias between the landers' pressure ob-
 702 servations is largely due to different landing elevations. Detailed investigation reveals
 703 that during L_s 0 – 170° the Perseverance pressure looks to be decreasing somewhat
 704 more slowly than the pressure measured by the historical Viking landers. However,
 705 Insight exhibits similar kind of slow pressure decrease and hence this could be due to
 706 a regional occurrence possibly related with the regional topography or variability in
 707 large scale atmospheric flows.

708 The observed diurnal pressure amplitude is ranging roughly within 2 -5 % of
 709 the sol-averaged pressure with the absolute amplitude (10 – 35 hPa) not having a
 710 direct relationship with the sol-averaged pressure. The optical thickness varying
 711 with the amount of airborne dust seems to affect considerably the diurnal pressure
 712 amplitude. The increase of optical thickness from 0.5 to 0.8 around sols 130-160

713 seems to raise the diurnal pressure amplitude from approximately 20 hPa to 35 hPa.
 714 Regional atmospheric models seem to give roughly similar results on the average
 715 diurnal pressure amplitude, when Perseverance -like airborne dust conditions are
 716 assumed.

717 It appears to be evident that the range of diurnal atmospheric pressure varies
 718 considerably with location on Mars. The Perseverance diurnal pressure variation
 719 seem to be smaller than those measured by the Curiosity rover at Gale crater where
 720 tidal forcing is stronger due to the location close to the equator and also due to the
 721 fact that at Curiosity's longitude sector eastward and westward modes are expected
 722 to interact constructively. Comparison with pressure observations at other Martian
 723 sites it looks that also regional and local geography also play a role in the range of
 724 observed diurnal pressure variation.

725 When inspecting the structure of diurnal pressure, 2-4 small peaks appear
 726 in the data on each sol (Figure 6). A clear evolution of the peaks can be seen in
 727 the stacked diurnal pressure data. During Northern summer (Figure 6, second row
 728 from top) diurnal pressure exhibits two distinct and regular peaks, one in the morn-
 729 ing around 6-7 AM and the other one around 8-9 PM LTST. During the Northern
 730 spring (Figure 6, top row) and fall (Figure 6, lowest rows) this summertime regular
 731 pattern is broken into more like four separate peaks whose amplitudes vary along
 732 with advancing season.

733 During Northern springtime - at the start of the mission, Perseverance sols
 734 0-150 - it appears that smaller peaks are superimposed on the larger peaks. These
 735 smaller peaks disappear between about sols 150 and 250 (Northern summertime)
 736 and return around sol 300 in early fall. The wintertime has not yet come during the
 737 first 414 Perseverance sols. The features in the plots give clues on the behaviour of
 738 regional atmospheric dynamics and circulation patterns in the Martian atmosphere

739 The daily surface pressure profile seems to exhibit a largely repeatable two-
 740 peak shape during the Northern summertime (Figure 6). This is probably mostly
 741 due to the strong semi-diurnal thermal tidal component, which seems to be the case
 742 as illustrated in Figure 7.

743 MEDA PS observations allow us to estimate that about 100 thermal vor-
 744 tices with ≈ 0.5 Pa pressure drops during a 20 sol period throughout the first 414
 745 Perseverance sols. Based on this analysis, the vortex activity at Jezero crater in
 746 the vicinity of Perseverance seems to be nearly constant with little seasonal vari-
 747 ation. Apparently solar forcing varying considerably from springtime to fall has
 748 not affected the frequency of occurrence of thermal vortices. It is interesting to see
 749 whether this pattern will hold through the upcoming Northern wintertime.

750 Through *in situ* pressure observations and regional atmospheric modeling re-
 751 sults a distinct local circulation pattern including nighttime katabatic and daytime
 752 upslope flows over the boundary of the Jezero crater was discovered. This circulation
 753 amplifies the diurnal pressure variation.

754 For comparison, the Gale crater diurnal pressure amplitude measured by the
 755 Curiosity Rover is much larger (50 to 120 hPa) than at the Jezero crater. This
 756 may be due to the fact that Gale is smaller and deeper than Jezero resulting in a
 757 stronger diurnal pressure cycle due to hydrostatic adjustment. On the plateaus with
 758 more gentle local circulation the diurnal pressure variation based on Viking Lander
 759 observations is weaker than at the Gale crater and about the same as given by Per-
 760 severance observations. On the other hand Insight diurnal pressure is higher than
 761 that of Perseverance during Northern springtime and summer but assumes roughly
 762 the same level during fall. Apparently the behavior of local diurnal pressure is af-

763 fected by a mixture of solar forcing on the surface, airborne dust, regional geography
764 and atmospheric wave activity.

765 The observed diurnal pressure variation seems to have a significant seasonal
766 dependence. During Northern summer diurnal pressure displays two distinct and
767 regular peaks, one in the morning around 6-7 AM and the other one around 8-9 PM
768 LTST. This regular pattern is likely caused by the interaction of strong thermal tide
769 and the seasonally varying airborne dust causing an amplified semi-diurnal compo-
770 nent. During the Northern fall and spring this summertime regular pattern is broken
771 into four separate peaks whose amplitudes vary along with advancing season.

772 The seasonal form of the diurnal pressure variation was investigated through
773 regional atmospheric modeling by Mars WRF and MRAMS limited area models us-
774 ing the modeling results described in Pla-Garcia et al. (2020). The modeling results
775 were compared with actual MEDA PS observations at solar longitude values L_s 0° ,
776 90° and 180° , as well as with the MCD data. In the summertime (midsummer
777 L_s 90°) the modeling results match very well with the shape and two-peak pattern
778 of diurnal pressure cycle, but they underestimate the average pressure level. These
779 modeling results showed the importance of the boundary fields for the regional mod-
780 els in getting pressure levels correct. Also the complexity of the diurnal pressure
781 signal especially during the springtime and fall was revealed.

782 Overall, the modeling data seems to fit surprisingly well with the Perseverance
783 pressure observations. Mars WRF and MRAMS have higher resolution than the
784 relatively coarse MCD and hence these models pick up the local daily pressure vari-
785 ation better than MCD. But even the MCD seems to work surprisingly well, which
786 is an excellent indication of the capabilities of current Martian atmospheric modeling
787 tools. The modelling data indicates that they are correctly modelling the large-scale
788 forcing of the main components of the daily pressure curves.

789 These modeling efforts underlined the clear need to investigate more in detail
790 the diurnal pressure cycle as a superposition of the thermal tide, regional and local
791 crater circulations and of various barotropic and baroclinic wave forms with seasonal
792 dependence. These differences between the models and the observations inform us
793 about the needs and areas to focus on in improving atmospheric models.

794 8 Open Research

795 The observational data used for this work is available in Planetary Data Sys-
796 tem (PDS) at the web site <https://pds.nasa.gov/>. MEDA instrument data is avail-
797 able in the PDS Atmospheres node in <https://doi.org/10.17189/1522849> (Rodriguez-
798 Manfredi & de la Torre Juarez, 2021).

799 Acknowledgments

800 Ari-Matti Harri, Mark Paton, Maria Hieta and Jouni Polkko are thankful
801 for the Finnish Academy grant number 310509. Agustín Sánchez-Lavega and
802 Ricardo Hueso were supported by Grant PID2019-109467GB-I00 funded by
803 MCIN/AEI/10.13039/501100011033/ and by Grupos Gobierno Vasco IT1742-22.

References

- 804
- 805 Barnes, J. R., Pollack, J. B., Haberle, R. M., Leovy, C. B., Zurek, R. W., Lee, H., &
806 Schaeffer, J. (1993). Mars atmospheric dynamics as simulated by the NASA
807 Ames General Circulation Model, 2, transient baroclinic eddies. *J. Geophys.*
808 *Res.*, *98*, 3125–3148.
- 809 Basu, S., Richardson, M. I., & Wilson, R. J. (2004, November). Simulation of
810 the Martian dust cycle with the GFDL Mars GCM. *Journal of Geophysical*
811 *Research (Planets)*, *109*(E11), E11006. doi: 10.1029/2004JE002243
- 812 Battalio, J. M., & Lora, J. M. (2021, August). Annular modes of variability in the
813 atmospheres of Mars and Titan. *Nature Astronomy*, *5*, 1139–1147. doi: 10
814 .1038/s41550-021-01447-4
- 815 Ferri, F., Smith, P. H., Lemmon, M., & Rennó, N. O. (2003, December). Dust dev-
816 ils as observed by Mars Pathfinder. *Journal of Geophysical Research (Planets)*,
817 *108*(E12), 5133. doi: 10.1029/2000JE001421
- 818 Forget, F., Hourdin, F., Fournier, R., Hourdin, C., Talagrand, O., Collins, M., ...
819 Huot, J.-P. (1999, October). Improved general circulation models of the Mar-
820 tian atmosphere from the surface to above 80 km. *J. Geophys. Res.*, *104*,
821 24155–24176. doi: 10.1029/1999JE001025
- 822 Golombek, M., Williams, N., Warner, N. H., Parker, T., Williams, M. G., Daubar,
823 I., ... Sklyanskiy, E. (2020, October). Location and Setting of the Mars In-
824 Sight Lander, Instruments, and Landing Site. *Earth and Space Science*, *7*(10),
825 e01248. doi: 10.1029/2020EA001248
- 826 Golombek, M. P., Bridges, N. T., Moore, H. J., Murchie, S. L., Murphy, J. R.,
827 Parker, T. J., ... Wilson, G. R. (1999, April). Overview of the Mars
828 Pathfinder Mission: Launch through landing, surface operations, data
829 sets, and science results. *J. Geophys. Res.*, *104*(E4), 8523–8554. doi:
830 10.1029/98JE02554
- 831 Gómez-Elvira, J., Armiens, C., Castañer, L., Domínguez, M., Genzer, M., Gómez,
832 F., ... Martín-Torres, J. (2012, September). REMS: The Environmental
833 Sensor Suite for the Mars Science Laboratory Rover. *Space Sci. Rev.*, *170*,
834 583–640. doi: 10.1007/s11214-012-9921-1
- 835 Guo, X., Lawson, W. G., Richardson, M. I., & Toigo, A. (2009, July). Fitting
836 the Viking lander surface pressure cycle with a Mars General Circulation
837 Model. *Journal of Geophysical Research (Planets)*, *114*(E7), E07006. doi:
838 10.1029/2008JE003302
- 839 Guzewich, S. D., Newman, C. E., de la Torre Juárez, M., Wilson, R. J., Lemmon,
840 M., Smith, M. D., ... Harri, A. M. (2016, April). Atmospheric tides in Gale
841 Crater, Mars. *Icarus*, *268*, 37–49. doi: 10.1016/j.icarus.2015.12.028
- 842 Haberle, Houben, H. C., Hertenstein, R., & Herdtle, T. (1993, June). A boundary-
843 layer model for Mars - Comparison with Viking lander and entry data. *J. At-*
844 *mos. Sci.*, *50*, 1544–1559. doi: 10.1175/1520-0469(1993)050<1544:ABLMFM>2.0
845 .CO;2
- 846 Haberle, R. M., Gómez-Elvira, J., de la Torre Juárez, M., Harri, A.-M.,
847 Hollingsworth, J. L., Kahanpää, H., ... Teams, R. S. (2014). Preliminary
848 interpretation of the remps pressure data from the first 100 sols of the msl mis-
849 sion. *Journal of Geophysical Research: Planets*, *119*(3), 440–453. Retrieved
850 from [https://agupubs.onlinelibrary.wiley.com/doi/abs/10.1002/](https://agupubs.onlinelibrary.wiley.com/doi/abs/10.1002/2013JE004488)
851 [2013JE004488](https://doi.org/10.1002/2013JE004488) doi: <https://doi.org/10.1002/2013JE004488>
- 852 Harri, A. M., Genzer, M., Kempainen, O., Kahanpää, H., Gomez-Elvira, J.,
853 Rodriguez-Manfredi, J. A., ... REMS/MSL Science Team (2014, January).
854 Pressure observations by the Curiosity rover: Initial results. *Journal of Geo-*
855 *physical Research (Planets)*, *119*(1), 82–92. doi: 10.1002/2013JE004423
- 856 Hess, S. L., Ryan, J. A., Tillman, J. E., Henry, R. M., & Leovy, C. B. (1980,
857 March). The annual cycle of pressure on Mars measured by Viking landers
858 1 and 2. *Geophys. Res. Lett.*, *7*, 197–200. doi: 10.1029/GL007i003p00197

- 859 Hourdin, F., Le van, P., Forget, F., & Talagrand, O. (1993, November). Meteorological
860 Variability and the Annual Surface Pressure Cycle on Mars. *Journal of At-*
861 *mospheric Sciences*, *50*(21), 3625-3640. doi: 10.1175/1520-0469(1993)050<3625:
862 MVATAS>2.0.CO;2
- 863 Hueso, R., Newman, C. E., del Río-Gaztelurrutia, T., Munguira, A., Sánchez-
864 Lavega, A., Toledo, D., ... Lepinette-Malvite, A. (2023). Convective vortices
865 and dust devils detected and characterized by mars 2020. *Journal of Geophys-*
866 *ical Research: Planets*, *128*(2), e2022JE007516. Retrieved from [https://](https://agupubs.onlinelibrary.wiley.com/doi/abs/10.1029/2022JE007516)
867 agupubs.onlinelibrary.wiley.com/doi/abs/10.1029/2022JE007516
868 (e2022JE007516 2022JE007516) doi: <https://doi.org/10.1029/2022JE007516>
- 869 James, P. B., Kieffer, H. H., & Paige, D. A. (1992). The seasonal cycle of car-
870 bon dioxide on Mars. In H. H. Kieffer, B. M. Jakosky, C. W. Snyder, &
871 M. S. Matthews (Eds.), *Mars* (p. 934-968). University of Arizona Press.
- 872 Kahre, M. A., & Haberle, R. M. (2010, June). Mars CO₂ cycle: Effects of airborne
873 dust and polar cap ice emissivity. *Icarus*, *207*, 648-653.
- 874 Kieffer, H. H., Chase, S. C., Miner, E. D., Munch, G., & Neugebauer, G. (1973).
875 Preliminary report on infrared radiometric measurements from the Mariner 9
876 spacecraft. *J. Geophys. Res.*, *78*, 4291-4312.
- 877 Kieffer, H. H., Jakosky, B. M., Snyder, C. W., & Matthews, M. S. (Eds.). (1992).
878 *Mars*. University of Arizona Press.
- 879 Kieffer, H. H., Martin, T. Z., Peterfreund, A. R., Jakosky, B. M., Miner, E. D., &
880 Palluconi, F. D. (1977). Thermal and albedo mapping of Mars during the
881 Viking primary mission. *J. Geophys. Res.*, *82*, 4249-4291.
- 882 Kliore, A., Cain, D. L., Fjeldbo, G., Seidel, B. L., Sykes, M. J., & Woiceshyn, P. M.
883 (1973, March). Some Recent Results of Mariner 9 Occultation Measurements
884 of Mars. In *Bulletin of the american astronomical society* (Vol. 5, p. 298).
- 885 Kliore, A., Cain, D. L., Levy, G. S., Eshleman, V. R., Fjeldbo, G., & Drake, F. D.
886 (1965, September). Occultation Experiment: Results of the First Direct
887 Measurement of Mars's Atmosphere and Ionosphere. *Science*, *149*(3689),
888 1243-1248. doi: 10.1126/science.149.3689.1243
- 889 Kliore, A., Fjeldbo, G., Seidel, B. L., & Rasool, S. I. (1969, December). Mariners 6
890 and 7: Radio Occultation Measurements of the Atmosphere of Mars. *Science*,
891 *166*(3911), 1393-1397. doi: 10.1126/science.166.3911.1393
- 892 Lee, C., Lawson, W. G., Richardson, M. I., Anderson, J. L., Collins, N., Hoar, T.,
893 & Mischna, M. (2011, November). Demonstration of ensemble data assimi-
894 lation for Mars using DART, MarsWRF, and radiance observations from MGS
895 TES. *Journal of Geophysical Research (Planets)*, *116*(E11), E11011. doi:
896 10.1029/2011JE003815
- 897 Lemmon, M. T., Smith, M. D., Viudez-Moreiras, D., de la Torre-Juarez, M.,
898 Vicente-Retortillo, A., Munguira, A., ... Apestigue, V. (2022). Dust,
899 sand, and winds within an active martian storm in jezero crater. *Geophys-*
900 *ical Research Letters*, *49*(17), e2022GL100126. Retrieved from [https://](https://agupubs.onlinelibrary.wiley.com/doi/abs/10.1029/2022GL100126)
901 agupubs.onlinelibrary.wiley.com/doi/abs/10.1029/2022GL100126
902 (e2022GL100126 2022GL100126) doi: <https://doi.org/10.1029/2022GL100126>
- 903 Leovy, C. B., & Mintz, Y. (1969). Numerical simulation of the atmospheric circula-
904 tion and climate of Mars. *J. Geophys. Res.*, *26*, 1167-1190.
- 905 LMD-Jussieu. (2021). *Mcd - mars climate database*. Retrieved from [http://www](http://www-mars.lmd.jussieu.fr/)
906 [-mars.lmd.jussieu.fr/](http://www-mars.lmd.jussieu.fr/) (Accessed = 2022-8-26)
- 907 Montabone, L., Forget, F., Millour, E., Wilson, R. J., Lewis, S. R., Cantor, B.,
908 ... Wolff, M. J. (2015). Eight-year climatology of dust optical depth on
909 mars. *Icarus*, *251*, 65-95. (Dynamic Mars) doi: [https://doi.org/10.1016/](https://doi.org/10.1016/j.icarus.2014.12.034)
910 [j.icarus.2014.12.034](https://doi.org/10.1016/j.icarus.2014.12.034)
- 911 Montabone, L., Marsh, K., Lewis, S. R., Read, P. L., Smith, M. D., Holmes, J.,
912 ... Pamment, A. (2014). The mars analysis correction data assimilation
913 (macda) dataset v1.0. *Geoscience Data Journal*, *1*(2), 129-139. Retrieved from

- 914 <https://rmetsonline.wiley.com/doi/abs/10.1002/gdj3.13> doi:
915 <https://doi.org/10.1002/gdj3.13>
- 916 Newman, C., Bertrand, T., Battalio, J., Day, M., De La Torre Juárez, M., Elrod,
917 M. K., . . . Zorzano, M.-P. (2021, May). Toward More Realistic Simulation and
918 Prediction of Dust Storms on Mars. In *Bulletin of the american astronomical*
919 *society* (Vol. 53, p. 278). doi: 10.3847/25c2cfeb.726b0b65
- 920 Newman, C., Juárez, M., Pla-García, J., Wilson, R., Lewis, S., Neary, L., . . .
921 Rodríguez-Manfredi, J. (2021, 02). Multi-model meteorological and aeolian
922 predictions for mars 2020 and the jezero crater region. *Space Science Reviews*,
923 *217*. doi: 10.1007/s11214-020-00788-2
- 924 Newman, C. E., Gómez-Elvira, J., Marin, M., Navarro, S., Torres, J., Richard-
925 son, M. I., . . . Bridges, N. T. (2017, July). Winds measured by the
926 Rover Environmental Monitoring Station (REMS) during the Mars Sci-
927 ence Laboratory (MSL) rover’s Bagnold Dunes Campaign and compari-
928 son with numerical modeling using MarsWRF. *Icarus*, *291*, 203-231. doi:
929 10.1016/j.icarus.2016.12.016
- 930 Newman, C. E., Hueso, R., Lemmon, M. T., Munguira, A., Álvaro Vicente-
931 Retortillo, Apestigue, V., . . . Guzewich, S. D. (2022). The dynamic atmo-
932 spheric and aeolian environment of jezero crater, mars. *Science Advances*,
933 *8*(21), eabn3783. Retrieved from [https://www.science.org/doi/abs/](https://www.science.org/doi/abs/10.1126/sciadv.abn3783)
934 [10.1126/sciadv.abn3783](https://www.science.org/doi/abs/10.1126/sciadv.abn3783) doi: 10.1126/sciadv.abn3783
- 935 Newman, C. E., Lee, C., Mischna, M. A., Richardson, M. I., & Shirley, J. H. (2019,
936 January). An initial assessment of the impact of postulated orbit-spin coupling
937 on Mars dust storm variability in fully interactive dust simulations. *Icarus*,
938 *317*, 649-668. doi: 10.1016/j.icarus.2018.07.023
- 939 Paige, D. A., & Ingersoll, A. P. (1985, June). Annual Heat Balance of Martian Po-
940 lar Caps: Viking Observations. *Science*, *228*(4704), 1160-1168. doi: 10.1126/
941 science.228.4704.1160
- 942 Pollack, J. B., Haberle, R. M., Schaeffer, J., & Lee, H. (1990). Simulations of the
943 general circulation of the Martian atmosphere 1. polar processes. *J. Geophys.*
944 *Res.*, *95*, 1447–1473.
- 945 Pollack, J. B., Leovy, C. B., Greiman, P. W., & Mintz, Y. (1981). A Martian general
946 circulation experiment with large topography. *J. Atmos. Sci.*, *38*, 3–29.
- 947 Rafkin, S. C. R., Pla-Garcia, J., Kahre, M., Gomez-Elvira, J., Hamilton, V. E.,
948 Marín, M., . . . Vasavada, A. (2016, December). The meteorology of Gale
949 Crater as determined from Rover Environmental Monitoring Station observa-
950 tions and numerical modeling. Part II: Interpretation. *Icarus*, *280*, 114-138.
951 doi: 10.1016/j.icarus.2016.01.031
- 952 Read, P., & Lewis, S. (2004). *The martian climate revisited - atmosphere and envi-*
953 *ronment of a desert planet*. Springer.
- 954 Richardson, M. I., & Newman, C. E. (2018, December). On the relationship be-
955 tween surface pressure, terrain elevation, and air temperature. Part I: The
956 large diurnal surface pressure range at Gale Crater, Mars and its origin due
957 to lateral hydrostatic adjustment. *Planet. Space Sci.*, *164*, 132-157. doi:
958 10.1016/j.pss.2018.07.003
- 959 Richardson, M. I., Toigo, A. D., & Newman, C. E. (2007). PlanetWRF: A gen-
960 eral purpose, local to global numerical model for planetary atmospheric and
961 climate dynamics. *J. Geophys. Res.*, *112*, 9001. doi: 10.1029/2006JE002825
- 962 Rodríguez-Manfredi, J. A., de la Torre Juárez, M., Alonso, A., Apéstigue, V.,
963 Arruego, I., Atienza, T., . . . MEDA Team (2021, April). The Mars
964 Environmental Dynamics Analyzer, MEDA. A Suite of Environmental
965 Sensors for the Mars 2020 Mission. *Space Sci. Rev.*, *217*(3), 48. doi:
966 10.1007/s11214-021-00816-9
- 967 Rodríguez-Manfredi, J. A., & de la Torre Juárez, M. (2021). *Mars 2020 meda bundle*
968 *dataset*. (NASA. Retrievable from <https://doi.org/10.17189/1522849>)

- 969 Rogberg, P., Read, P. L., Lewis, S. R., & Montabone, L. (2010, August). Assess-
 970 ing atmospheric predictability on Mars using numerical weather prediction
 971 and data assimilation. *Quarterly Journal of the Royal Meteorological Society*,
 972 *136*(651), 1614-1635. doi: 10.1002/qj.677
- 973 Savijärvi, H., & Kauhanen, J. (2008, April). Surface and boundary-layer modelling
 974 for the mars exploration rover sites. *Quarterly J. Royal Met. Soc.*, *134*, 635-
 975 641. doi: 10.1002/qj.232
- 976 Savijärvi, H., & Määttänen, A. (2010, August). Boundary-layer simulations for the
 977 Mars Phoenix lander site. *Quarterly J. Royal Met. Soc.*, *136*, 1497-1505. doi:
 978 10.1002/qj.650
- 979 Schofield, J. T., Barnes, J. R., Crisp, D., Haberle, R. M., Larsen, S., Magalhaes,
 980 J. A., ... Wilson, G. (1997, December). The Mars Pathfinder Atmo-
 981 spheric Structure Investigation/Meteorology. *Science*, *278*, 1752. doi:
 982 10.1126/science.278.5344.1752
- 983 Smith, D. E., Zuber, M. T., Frey, H. V., Garvin, J. B., Head, J. W., Muhleman,
 984 D. O., ... Sun, X. (2001, October). Mars Orbiter Laser Altimeter: Experiment
 985 summary after the first year of global mapping of Mars. *J. Geophys. Res.*,
 986 *106*(E10), 23689-23722. doi: 10.1029/2000JE001364
- 987 Snyder, C. W., & Moroz, V. I. (1992). Spacecraft exploration of Mars. In H. H. Ki-
 988 effer, B. M. Jakosky, C. W. Snyder, & M. S. Matthews (Eds.), *Mars* (p. 71-
 989 119). University of Arizona Press.
- 990 Soffen, G. A. (1976, December). Scientific results of the Viking missions. *Science*,
 991 *194*, 1274-1276. doi: 10.1126/science.194.4271.1274
- 992 Soffen, G. A. (1977, September). The viking project. *J. Geophys. Res.*, *82*, 3959-
 993 3970. doi: 10.1029/JS082i028p03959
- 994 Sánchez-Lavega, A., del Rio-Gaztelurrutia, T., Hueso, R., Juárez, M. d. l. T.,
 995 Martínez, G. M., Harri, A.-M., ... Mäkinen, T. (2023). Mars 2020 persever-
 996 ance rover studies of the martian atmosphere over jezero from pressure mea-
 997 surements. *Journal of Geophysical Research: Planets*, *128*(1), e2022JE007480.
 998 Retrieved from [https://agupubs.onlinelibrary.wiley.com/doi/abs/](https://agupubs.onlinelibrary.wiley.com/doi/abs/10.1029/2022JE007480)
 999 [10.1029/2022JE007480](https://doi.org/10.1029/2022JE007480) (e2022JE007480 2022JE007480) doi: [https://doi.org/](https://doi.org/10.1029/2022JE007480)
 1000 [10.1029/2022JE007480](https://doi.org/10.1029/2022JE007480)
- 1001 Taylor, P. A., Catling, D. C., Daly, M., Dickinson, C. S., Gunnlaugsson, H. P.,
 1002 Harri, A.-M., & Lange, C. F. (2008, July). Temperature, pressure, and wind
 1003 instrumentation in the Phoenix meteorological package. *J. Geophys. Res.*, *113*,
 1004 0. doi: 10.1029/2007JE003015
- 1005 Tillman, J. E. (1988, August). Mars global atmospheric oscillations - Annually syn-
 1006 chronized, transient normal-mode oscillations and the triggering of global dust
 1007 storms. *J. Geophys. Res.*, *93*, 9433-9451. doi: 10.1029/JD093iD08p09433
- 1008 Tillman, J. E., Henry, R. M., & Hess, S. L. (1979, June). Frontal systems dur-
 1009 ing passage of the Martian north polar HOOD over the Viking Lander 2 site
 1010 prior to the first 1977 dust storm. *J. Geophys. Res.*, *84*, 2947-2955. doi:
 1011 10.1029/JB084iB06p02947
- 1012 Tillman, J. E., Johnson, N. C., Guttorp, P., & Percival, D. B. (1994). Erratum:
 1013 "The Martian annual atmospheric pressure cycle: Years without great dust
 1014 storms" [*J. Geophys. Res.*, *98*(E6), 10,963-10,971 (1993)]. *J. Geophys. Res.*, *99*,
 1015 3813-3814. doi: 10.1029/94JE00232
- 1016 Toigo, A. D., & Richardson, M. I. (2003, November). Meteorology of proposed
 1017 Mars Exploration Rover landing sites. *Journal of Geophysical Research (Plan-*
 1018 *ets)*, *108*(E12), 8092. doi: 10.1029/2003JE002064
- 1019 Wilson, R. J., & Hamilton, K. (1996, May). Comprehensive model simulation of
 1020 thermal tides in the Martian atmosphere. *Journal of Atmospheric Sciences*,
 1021 *53*(9), 1290-1326. doi: 10.1175/1520-0469(1996)053<1290:CMSOTT>2.0.CO;2
- 1022 Young, L. D. G. (1969, November). Interpretation of High-Resolution Spectra of
 1023 Mars. I. CO₂ Abundance and Surface Pressure Derived from the Curve of

- 1024 Growth. *icarus*, 11(3), 386-389. doi: 10.1016/0019-1035(69)90070-0
- 1025 Zurek, R. W. (1978, August). Solar heating of the Martian dusty atmosphere.
- 1026 *Icarus*, 35, 196-208. doi: 10.1016/0019-1035(78)90005-2
- 1027 Zurek, R. W. (1981, January). Inference of dust opacities for the 1977 Martian great
- 1028 dust storms from Viking Lander 1 pressure data. *Icarus*, 45, 202-215. doi: 10
- 1029 .1016/0019-1035(81)90014-2
- 1030 Zurek, R. W. (1982, June). Martian great dust storms - an update. *Icarus*, 50, 288-
- 1031 310. doi: 10.1016/0019-1035(82)90127-0
- 1032 Zurek, R. W. (1992). Comparative aspects of the climate of Mars: an introduction
- 1033 to the current atmosphere. In H. H. Kieffer, B. M. Jakosky, C. W. Snyder, &
- 1034 M. S. Matthews (Eds.), *Mars* (p. 799-817). University of Arizona Press.
- 1035 Zurek, R. W., Barnes, J. R., Haberle, R. M., Pollack, J. B., Tillman, J. E., & Leovy,
- 1036 C. B. (1992a). Dynamics of the atmosphere of Mars. In H. H. Kieffer,
- 1037 B. M. Jakosky, C. W. Snyder, & M. S. Matthews (Eds.), *Mars* (p. 835-934).
- 1038 University of Arizona Press.
- 1039 Zurek, R. W., Barnes, J. R., Haberle, R. M., Pollack, J. B., Tillman, J. E., & Leovy,
- 1040 C. B. (1992b). Dynamics of the atmosphere of Mars. In H. H. Kieffer,
- 1041 B. M. Jakosky, C. W. Snyder, & M. S. Matthews (Eds.), *Mars* (p. 835-934).
- 1042 University of Arizona Press.